

THE HERSCHEL ATLAS

S. EALES¹, L. DUNNE², D. CLEMENTS³, A. COORAY⁴, G. DE ZOTTI⁵, S. DYE¹, R. IVISON⁶, M. JARVIS⁷, G. LAGACHE⁸, S. MADDOX², M. NEGRELLO⁹, S. SERJEANT⁹, M.A. THOMPSON⁷, E. VAN KAMPEN¹⁰, A. AMBLARD⁴, P. ANDREANI¹⁰, M. BAES¹¹, A. BEELEN⁸, G.J. BENDO³, D. BENFORD¹², F. BERTOLDI⁴⁰, J. BOCK⁴⁷, D. BONFIELD⁷, A. BOSELLI¹⁴, C. BRIDGE¹³, V. BUAT¹⁴, D. BURGARELLA¹⁴, R. CARLBERG⁴⁸, A. CAVA¹⁵, P. CHANIAL³, S. CHARLOT¹⁶, N. CHRISTOPHER⁴⁵, P. COLES¹, L. CORTESE¹, A. DARIUSH¹, E. DA CUNHA¹⁷, G. DALTON¹⁸, L. DANESE¹⁹, H. DANNERBAUER²⁰, S. DRIVER⁴⁶, J. DUNLOP³¹, L. FAN¹⁹, D. FARRAH²¹, D. FRAYER²², C. FRENK²³, J. GEACH²³, J. GARDNER¹², H. GOMEZ¹, J. GONZÁLEZ-NUEVO¹⁹, E. GONZÁLEZ-SOLARES²⁴, M. GRIFFIN¹, M. HARDCASTLE⁷, E. HATZIMINAOGLOU¹⁰, D. HERRANZ²⁵, D. HUGHES²⁶, E. IBAR⁶, WOONG-SEOB JEONG³⁰, C. LACEY²³, A. LAPI⁵¹, M. LEE²⁷, L. LEEUW²⁸, J. LISKE¹⁰, M. LÓPEZ-CANIEGO²⁹, T. MÜLLER³⁰, K. NANDRA³, P. PANUZZO³⁹, A. PAPAGEORGIOU¹, G. PATANCHON⁴⁹, J. PEACOCK³¹, C. PEARSON³², S. PHILLIPPS³³, M. POHLEN¹, C. POPESCU³⁴, S. RAWLINGS⁴⁵, E. RIGBY², M. RIGOPOULOU¹⁸, G. RODIGHIERO⁴², A. SANSOM³⁴, B. SCHULZ¹³, D. SCOTT³⁵, D.J.B. SMITH², B. SIBTHORPE⁶, I. SMAIL²³, J. STEVENS⁷, W. SUTHERLAND³⁶, T. TAKEUCHI³⁷, J. TEDDS³⁸, P. TEMI²⁸, R. TUFFS⁴¹, M. TRICHAS³, M. VACCARI⁴², I. VALTCHANOV⁴³, P. VAN DER WERF⁴⁴, A. VERMA⁴⁵, J. VIERIA¹³, C. VLAHAKIS⁴⁴ & GLENN J. WHITE^{9,32}

Draft version September 2, 2018

ABSTRACT

The Herschel ATLAS is the largest open-time key project that will be carried out on the Herschel Space Observatory. It will survey 510 square degrees of the extragalactic sky, four times larger than all the other Herschel surveys combined, in five far-infrared and submillimetre bands. We describe the survey, the complementary multi-wavelength datasets that will be combined with the Herschel data, and the six major science programmes we are undertaking. Using new models based on a previous submillimetre survey of galaxies, we present predictions of the properties of the ATLAS sources in other wavebands.

Subject headings:

¹ School of Physics and Astronomy, Cardiff University, Queens Buildings, The Parade, Cardiff CF24 3AA, UK

² School of Physics and Astronomy, University of Nottingham, Nottingham, NG7 2RD, UK

³ Physics Department, Imperial College London, Prince Consort Road, London, SW7 2AZ, UK

⁴ Center for Cosmology, University of California, Irvine, CA 92697, USA

⁵ INAF-Osservatorio Astronomico di Padova, I-35122 Padova, and SISSA, I-34014 Trieste, Italy

⁶ UK Astronomy Technology Centre, Royal Observatory, Blackford Hill, Edinburgh EH9 3HJ, UK

⁷ Centre for Astrophysics Research, STR1, University of Hertfordshire, Hatfield, AL10 9AB, UK

⁸ Institut d'Astrophysique Spatiale (IAS), Btiment 121, F-91405 Orsay, France; and Universit Paris-Sud 11 and CNRS (UMR 8617), France

⁹ Dept. of Physics and Astronomy, The Open University, Milton Keynes, MK7 6AA, UK

¹⁰ European Southern Observatory, Karl-Schwarzschild-Str. 2, 85748 Garching bei München, Germany

¹¹ Sterrenkundig Observatorium, Universiteit Gent, Krijgslaan 281 S9, B-9000 Gent, Belgium

¹² Observational Cosmology Laboratory, Code 665, NASA's Goddard Space Flight Center, Greenbelt MD 20771, USA

¹³ California Institute of Technology, 1200 East California Blvd., Pasadena, CA 91125, USA

¹⁴ Laboratoire d'Astrophysique de Marseille, Observatoire Astronomique Marseille Provence, Aix-Marseille Universit, CNRS, France

¹⁵ Instituto de Astrofísica de Canarias, Calle Va Lctea, E38205, La Laguna, Esp

¹⁶ Institut d'Astrophysique de Paris, CNRS UMR7095 UPMC, 98 bis boulevard Arago, F-75014 Paris, France

¹⁷ Department of Physics, University of Crete, 71003 Heraklion, Greece

¹⁸ Astrophysics, University of Oxford, Oxford OX1 3RH and The Rutherford Appleton Laboratory, Chilton, Didcot, OX11 0QX

¹⁹ SISSA, Via Beirut 2-4, I-34014 Trieste, Italy

²⁰ Max Planck Institute for Astronomy, Knigstuhl 17, D-69117 Heidelberg, German

²¹ Astronomy Centre, University of Sussex, Brighton, UK

²² Infrared Processing and Analysis Center, California Institute of Technology 100-22, Pasadena, CA 91125, USA

²³ Institute for Computational Cosmology, Physics Dept, Durham University, South Road, Durham DH1 3LE

²⁴ Institute of Astronomy, University of Cambridge, Madingley Rd., Cambridge CB3 0HA, UK

²⁵ Instituto de Física de Cantabria (CSIC-UC), Santander, 39005, Spain

²⁶ Instituto Nacional de Astrofísica, Óptica y Electrónica (INAOE), Aptdo. Postal 51 y 216, Puebla, Mexico

²⁷ Astronomy Program, Department of Physics and Astronomy, Seoul National University, Seoul 151-742, KOREA

²⁸ Astrophysics Branch, NASA Ames Research Center, Mail Stop 245-6, Moffett Field, CA 94035, USA

²⁹ Instituto de Física de Cantabria (CSIC-UC), Santander, 39005, Spain

³⁰ Max-Planck-Institut für extraterrestrische Physik, Giessenbachstrasse, 85748 Garching, Germany

³¹ Institute for Astronomy, University of Edinburgh, Royal Observatory, Edinburgh EH9 3HJ, UK

³² Rutherford Appleton Laboratory, Chilton, Didcot, Oxfordshire OX11 0QX, UK

³³ Astrophysics Group, Department of Physics, University of Bristol, Tyndall Avenue, Bristol BS8 1TL

³⁴ Jeremiah Horrocks Institute, University of Central Lancashire, Preston, PR1 2HE, UK

³⁵ Department of Physics & Astronomy, University of British Columbia, 6224 Agricultural Road, Vancouver BC, V6T1Z1, Canada

³⁶ Astronomy Unit, Queen Mary University of London, Mile End Road, London E1 4NS, UK

³⁷ Institute for Advanced Research, Nagoya University, Furocho, Chikusa-ku, Nagoya 464-8601, Japan

³⁸ Department of Physics and Astronomy, University of Leicester, University Road, Leicester LE1 7RH, UK

³⁹ CEA, Laboratoire AIM, Irfu/Sap, F-91191 Gif-sur-Yvette, France

⁴⁰ Argelander Institute for Astronomy, Bonn University, Auf dem Huegel 71, D-53121 Bonn, Germany

1. INTRODUCTION

Approximately half the energy emitted since the big bang by all the objects in the Universe has been absorbed by dust and then reradiated between 60 and 500 μm (Dwek et al. 1998; Fixsen et al. 1998; Driver et al. 2008), a wavelength range in which the Universe is still largely unexplored (Fig. 1). On the short-wavelength side of this waveband, the whole sky was surveyed at 60 and 100 μm by IRAS in the 1980s. However, almost all of the tens of thousands of galaxies detected by IRAS were spirals and starbursts in the nearby Universe ($z < 0.1$), and IRAS revealed little about the dust in other galaxy populations, especially early-type galaxies (Bregman et al. 1998). Even in the late-type galaxies, only the small fraction of the dust warm enough to radiate significantly in the far-infrared was detected by IRAS. Devereux and Young (1990), for example, showed that the gas-to-dust ratio estimated from IRAS measurements alone was ≈ 10 times greater than the standard Galactic value, implying that $\approx 90\%$ of the dust in galaxies was effectively missed by IRAS. ISO and Spitzer, with their long wavelength (170 μm) band, suffered less from this problem but will still have effectively missed any dust with $T < 15\text{K}$ (Bendo et al. 2003). Notwithstanding the successes of IRAS, ISO and Spitzer, most of the waveband from 60 to 500 μm is still virtually *terra incognita*, and the only survey of a large area of the extragalactic sky at a wavelength beyond 200 μm is the one recently carried out by the Herschel pathfinder experiment, the Balloon Large Area Survey Telescope (BLAST), which covers $\approx 20 \text{ deg}^2$ (Devlin et al. 2009).

The lack of a survey covering a large area of sky in the submillimetre waveband (in this paper defined as $100 \mu\text{m} < \lambda < 1 \text{ mm}$) has left us in some ways knowing more about dust in the distant, early Universe than in the Universe today. The surveys that have been carried out in the submillimetre waveband with ground-based telescopes—at 450 and 850 μm with the SCUBA camera on the James Clerk Maxwell Telescope (Hughes et al. 1998; Eales et al. 1999; Coppin et al. 2006), at 1.2 mm with MAMBO

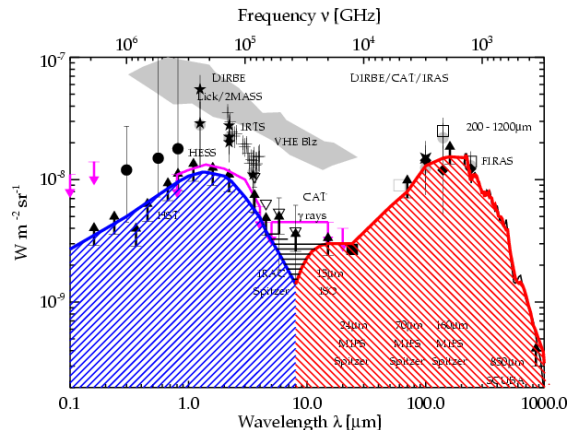


FIG. 1.— The extragalactic background radiation as a function of wavelength (Dole et al. 2006)

on the IRAM 30-m telescope (Greve et al. 2004; Bertoldi et al. 2007; Greve et al. 2008) and at 1.1 mm with AZTEC on the James Clerk Maxwell Telescope (Perera et al. 2008; Scott et al. 2008)—have been of very small areas of sky, covering $\sim 1 \text{ deg}^2$ of sky in total. Because of the unusual submillimetre ‘K-correction’⁵², these surveys have mostly detected sources at very high redshifts ($z \geq 1$). They have led to the important discovery that there is a population of luminous dust-enshrouded galaxies in the early Universe (Smail et al. 1997; Hughes et al. 1998), which many authors have suggested are the ancestors of ellipticals today (Scott et al. 2002; Dunne et al. 2003), but they have told us relatively little about the evolution of the Universe since $z \approx 1$ (the last 8 billion years) and almost nothing at all about dusty galaxies in the nearby Universe.

Two basic things one would like to know about the nearby Universe are the submillimetre luminosity function and the dust-mass function (the space-density of galaxies as a function of dust mass). These functions are important for many reasons, including tests of semi-analytical models of galaxy formation (Cole et al. 2000; Baugh et al. 2005) and, by comparison with the same functions at high redshift, accurate measurements of the amount of evolution that is occurring in the submillimetre waveband (Dunne et al. 2003). Unfortunately, our knowledge of these functions is still extremely poor because of the limitations in areal coverage and sensitivity of previous submillimetre telescopes. Until recently the only estimates of the local submillimetre luminosity function were one based on 55 galaxies detected in an ISO 170- μm survey (Takeuchi et al. 2006) and ones based on SCUBA 850- μm observations of ≈ 200 galaxies selected in other wavebands (Dunne et al. 2000; Vlahakis et al. 2005). There are now direct estimates from the BLAST results of the local luminosity function at 250, 350 and 500 μm (Eales et al. 2009), but their accuracy is limited by the small number of low-redshift sources detected in the BLAST survey: ≈ 30 at $z < 0.2$.

⁵² Beyond a redshift of ≈ 1 , as the redshift increases, the typical spectral energy distribution of a dusty galaxy means that the effect of increasing luminosity-distance on the brightness of the galaxy is compensated for by the increasing rest-frame luminosity of the galaxy. The consequence is that the galaxy’s flux density is approximately independent of redshift.

⁴¹ Max Planck Institut für Kernphysik, Saupfercheckweg 1, D-69117, Heidelberg, Germany

⁴² Department of Astronomy, University of Padova, Vicolo Osservatorio 3, I-35122, Padova, Italy

⁴³ Herschel Science Centre, ESA, P.O. Box 78, 28691 Villanueva de la Caada, Madrid, Spain

⁴⁴ Leiden Observatory, Leiden University, P.O. Box 9513, NL - 2300 RA Leiden, The Netherlands

⁴⁵ Oxford Astrophysics, Denys Wilkinson Building, University of Oxford, Keble Road, Oxford, OX1 3RH

⁴⁶ School of Physics and Astronomy, University of St Andrews, St Andrews, KY16 9SS

⁴⁷ Astrophysics and Space Science, Jet Propulsion Laboratory, Pasadena, CA, 91109, USA; and Department of Physics, Math and Astronomy, California Institute of Technology, Pasadena, CA, 91125, USA

⁴⁸ Department of Astronomy and Astrophysics, 50 St. George Street, Toronto, Ontario, M5S 3H4, Canada

⁴⁹ Université Denis Diderot, Laboratoire Astro-Particules et Cosmologie, 10 rue Alice Domon et Léonie Duquet, 75205, Paris Cedex 13, France

⁵⁰ Space Science Division, Korea Astronomy & Space Science Institute, 61-1, Whaam-dong, Yuseung-gu, Deajeon, 305-348, Republic of Korea

⁵¹ Physics Dept., University Tor Vergata, Via della Ricerca Scientifica 1, I-00133 Roma, Italy

The lack of a large-area survey capable of measuring the dust content and dust-obscured star formation in large numbers of galaxies in the local Universe has been especially galling for submillimetre astronomers in the light of the success of their colleagues working in other wavebands. The Sloan Digital Sky Survey and the 2dF Galaxy Redshift Survey have led to a revolution in our understanding of the distribution of galaxies in the local Universe, and the relationships between their present star-formation rate, star-formation history, stellar mass, morphology and environment (Lewis et al. 2002; Kauffmann et al. 2003a; Kauffmann et al. 2003b; Heavens et al. 2004; Balogh et al. 2004). However, all the studies that have used these impressive datasets to investigate the physics and ecology of the galaxy population have been forced to ignore the dust phase of the interstellar medium and star formation that is heavily obscured by dust, because the IRAS survey was only sensitive enough to detect a small percentage of the galaxies in the redshift surveys (1.8 per cent of the SDSS galaxies - Obric et al. 2006), and it missed 90% of the dust in the detected galaxies because of its insensitivity to cold dust (Devereux and Young 1990).

The launch of the Herschel Space Observatory, which occurred on May 14th 2009, has the potential to dramatically increase our knowledge of dust and dust-obscured star formation, especially in the nearby Universe. Herschel has two main cameras: SPIRE, which will be able to image the sky simultaneously at 250, 350 and 500 μm (Griffin et al. 2007), and PACS, which will be able to image the sky in two bands simultaneously, either 70 and 170 μm or 110 and 170 μm (Poglitsch et al. 2006). Herschel will have much better angular resolution ($\simeq 18$ arcsec at 250 μm) and sensitivity than previous observatories, and the spectral coverage of SPIRE will make it possible to carry out the first large-area surveys in this virtually unexplored part of the electromagnetic spectrum. The SPIRE bands will also make it possible to detect the cold dust that was missed by earlier observatories. Herschel is also better suited for investigating the local Universe than the submillimetre surveys that will soon be carried out from the ground, in particular the SCUBA-2 and LABOCA surveys, because these will operate mostly at 850 μm , where low-redshift galaxies are intrinsically faint, whereas the Herschel bands span the peak of the typical spectral energy distribution of a galaxy in the nearby Universe.

In this paper, we describe the largest project that will be carried out with the Herschel Space Observatory in ‘Open Time’, the time available for competition within the international astronomical community⁵³. The Herschel Astrophysical Terahertz Large Area Survey (the Herschel ATLAS or H-ATLAS) will be a survey of 510 deg² of sky in five photometric bands. This is $\simeq 8$ times larger than the coverage of the next largest (in area) Herschel extragalactic survey, HERMES (Oliver et al. 2009). The main scientific goal of the H-ATLAS is to provide measurements of the dust masses and dust-obscured star formation for tens of thousands of nearby galaxies, the far-IR/submillimetre equivalent to the SDSS photometric

⁵³ This forms about 2/3 of the total observing time on Herschel, with the remaining 1/3 being time reserved for the teams that built the instruments—‘Guaranteed Time’.

TABLE 1
H-ATLAS FIELDS

Name	Centre	RA width ^a	Dec width ^a
NGP	13 18 00, 29 00 00	15	10
GAMA A	09 00 00, 00 00 00	12	3
GAMA B	12 00 00, 00 00 00	12	3
GAMA C	14 30 00, 00 00 00	12	3
SGP A	02 26 48, -33 00 00	11	6
SGP B	23 15 36, -32 54 00	31	6

NOTE. — Reading from the left, the columns are: the name of the field; the central position of the field; the width of the field in degrees in RA; the width of the field in degrees in declination.

^a The precise coverage of the fields and their orientation on the sky will depend on exactly when they are observed. See §6 for more details.

survey. However, the H-ATLAS has many other science goals ranging from the investigation of the point sources that will be detected by the Planck Surveyor to a study of high-latitude galactic dust.

The arrangement of this paper is as follows. In Section 2 we describe the basic parameters of the survey. In Section 3 we present predictions of the number and redshift distribution of the sources that will be detected by the H-ATLAS. In Section 4, we describe the complementary data that exists or will soon exist for the H-ATLAS fields. In Section 5 we describe the six main H-ATLAS science programmes. In Section 6 we describe the detailed survey strategy, including issues that will be of interest to the general community, such as our plans for the release of data products. We everywhere assume the cosmological parameters for a ‘concordance universe’: $\Omega_{\text{M}} = 0.267$ and $\Omega_{\Lambda} = 0.762$.

2. THE BASIC PARAMETERS OF THE SURVEY

The H-ATLAS has been allocated 600 hours of time, making it the largest key project that will be carried out with Herschel in Open Time. For all of our science goals (§5), the final sensitivity of the survey is not critical and it is more important to survey the greatest possible area of sky. We have therefore chosen to use the maximum possible scan rate for the telescope (60 arcsec sec⁻¹). For our first science programme (§5.1), it is important to make observations with PACS and SPIRE, and therefore we have chosen to use the Herschel observing mode that allows simultaneous observations with the two cameras: Parallel Mode (PMode). Of the two possible combinations of photometric bands for PACS (Poglitsch et al. 2006), we have chosen to observe at 110 and 170 μm rather than at 70 and 170 μm mostly on the grounds of sensitivity; the noise at 70 and 110 μm should be fairly similar but galaxies, even at low redshift, are generally brighter at the longer wavelength. Although this combination will be worse for estimating the temperature of the dust, our models suggest that we will still be able to obtain useful measurements of the temperature of the dust in low-redshift galaxies.

With an eye on the legacy value of the H-ATLAS, we have chosen to observe fields in the northern and southern hemispheres and on the celestial equator. Other than that, we have chosen our fields to maximise the amount of complementary data and to minimize the amount of confusing emission from dust in the Galaxy, this last de-

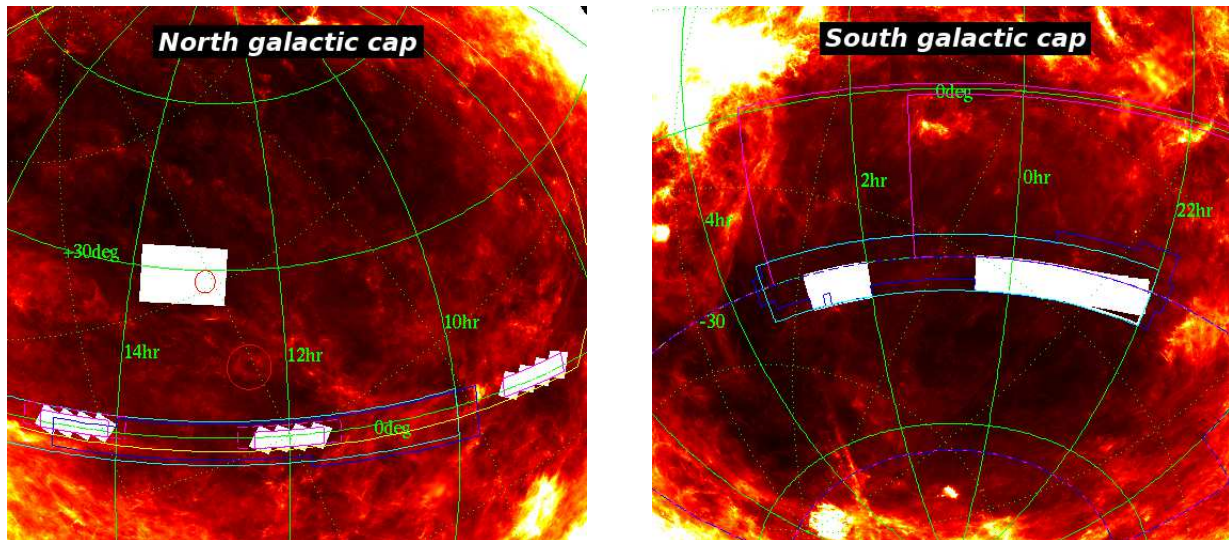


FIG. 2.— The positions of the ATLAS field, shown as white blocks, superimposed on the IRAS 100 μm map of the sky, which traces the distribution of galactic dust. Figure 2(a) shows the northern galactic cap and Figure 2(b) shows the southern galactic cap. The colour coding for the lines is as follow: solid green lines—RA and dec; dotted green lines—ecliptic latitude and longitude; cyan—KIDS/VIKING area; yellow—SDSS area; blue—2dFGRS area; magenta—area of the Dark Energy Survey; magenta/blue dashed—area covered by the South Pole Telescope.

terminated from the IRAS 100 μm maps. The fields, which are shown in Figure 2 and listed in Table 1, are:

- One field close to the northern galactic pole with an area of 150 deg^2 (henceforth the NGP field)
- Three fields, each of 36 deg^2 in area, coinciding with the fields being surveyed in the Galaxy And Mass Assembly redshift survey (Driver et al. 2009) (henceforth the GAMA fields)
- Two fields with a total area of 250 deg^2 close to the south galactic pole (henceforth the SGP fields)

The total survey covers 510 deg^2 . The angular resolution (full-width half maximum) of the observations will be approximately 8, 12, 18, 25 and 36 arcsec at 70, 110, 250, 350 and 500 μm , respectively. The 5σ sensitivities that should be reached in the five bands are 67 mJy at 110 μm , 94 mJy at 170 μm , 45 mJy at 250 μm , 62 mJy at 350 μm and 53 mJy at 500 μm . These sensitivities have been estimated using the current version of the Herschel observation planning package HSpot. We have assumed that the sources will be unresolved by the telescope beam, which will be true for most sources but will not be true for the closest sources. We have also neglected the effects of emission from dust in the Galaxy and of confusion from extragalactic sources. The importance of these is still uncertain, but the importance of confusion should be less than for the deeper Herschel surveys (Oliver et al. 2009).

3. PREDICTIONS

The number of sources that will be found in any of the Herschel surveys is uncertain because they cover regimes of flux density and wavelength that have never been explored before. There is a particular problem in the wavelength range $200 < \lambda < 500 \mu\text{m}$ because no survey, until the very recent survey with the balloon-borne telescope BLAST (Devlin et al. 2009), has been carried out

at these wavelengths. Models based on surveys at shorter wavelengths, such as IRAS, are likely to underestimate the number of sources in the submillimetre band because these surveys miss the cold dust that radiates strongly at the longer wavelengths (Dunne & Eales 2001).

We have used two models to predict the properties of the sources that will be found in the H-ATLAS. First, the model of Lagache and collaborators (Lagache et al. 2003; Lagache et al. 2004) is an empirical evolution model in which an analytical form is assumed for the evolution, and the parameters of the model are adjusted to fit the observational data in the far-infrared and submillimetre wavebands, in particular the source counts at 24, 70, 160 and 850 μm and the spectrum of the cosmic background radiation. Second, we have developed a new empirical evolution model based on the SCUBA Local Universe and Galaxy Survey (Dunne et al. 2000; Vlahakis et al. 2005). Both models give adequate agreement with the results of the BLAST survey (Dye et al. 2009), although the comparison between the results and the models is still at a preliminary stage because of the large amount of source confusion in the BLAST survey (Eales et al. 2009). We now describe the new model in more detail.

The model is based on the sample of 104 galaxies observed by Dunne et al. (2000) with the SCUBA submillimetre camera as part of the SCUBA Local Universe and Galaxy Survey (SLUGS). These galaxies form a statistically-complete sample above a flux limit at 60 μm of 5.24 Jy (Dunne et al. 2000). All of these galaxies were detected at 850 μm and many at 450 μm . Dunne and Eales (2001) present a simple two-component dust model that fits the 60, 100, 450 and 850 μm flux measurements. For the galaxies without measurements at 450 μm , it is possible to determine the parameters of the model by making the additional assumption that the temperature of the cold dust component is 20 K, which is the average of the estimates for the galaxies that do have complete flux measurements. The SLUGS sample is still the only large sample of galaxies for which there are

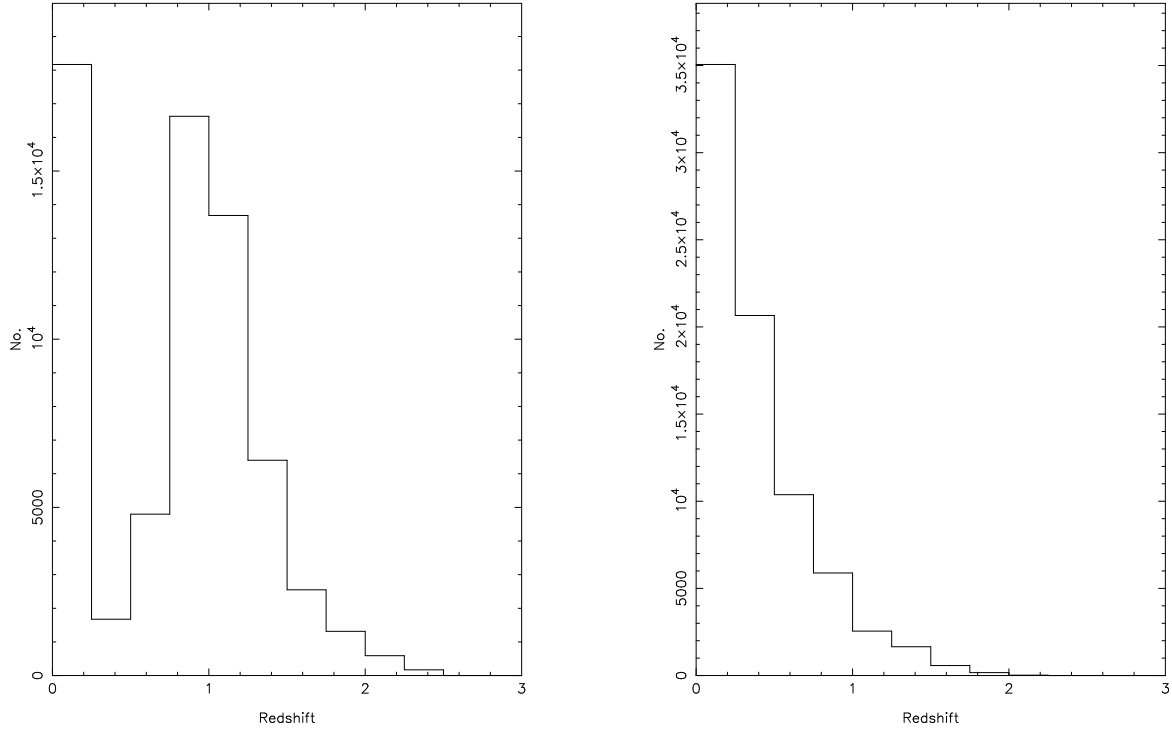


FIG. 3A.— On the left is the redshift distributions predicted at $110 \mu\text{m}$ by the models of Lagache et al. (2003,2004); on the right is the redshift distribution predicted at the same wavelength by the model described in the text.

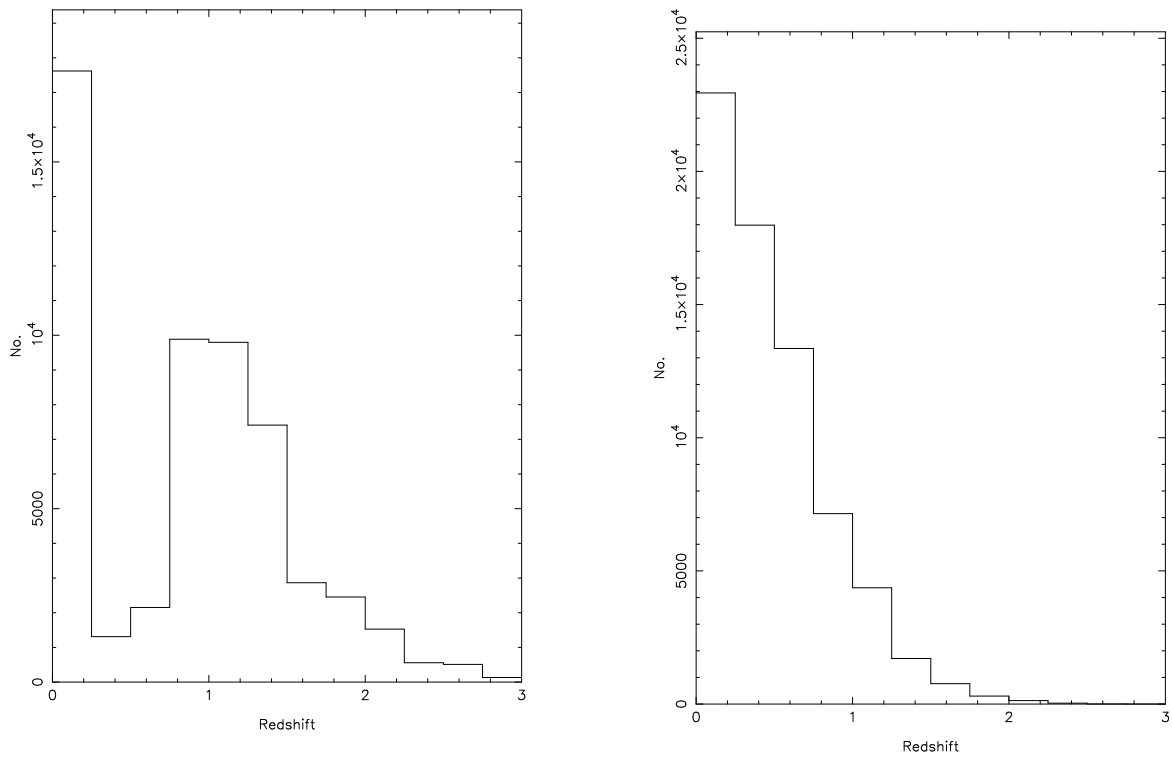


FIG. 3B.— Same as in (a) except at $170 \mu\text{m}$.

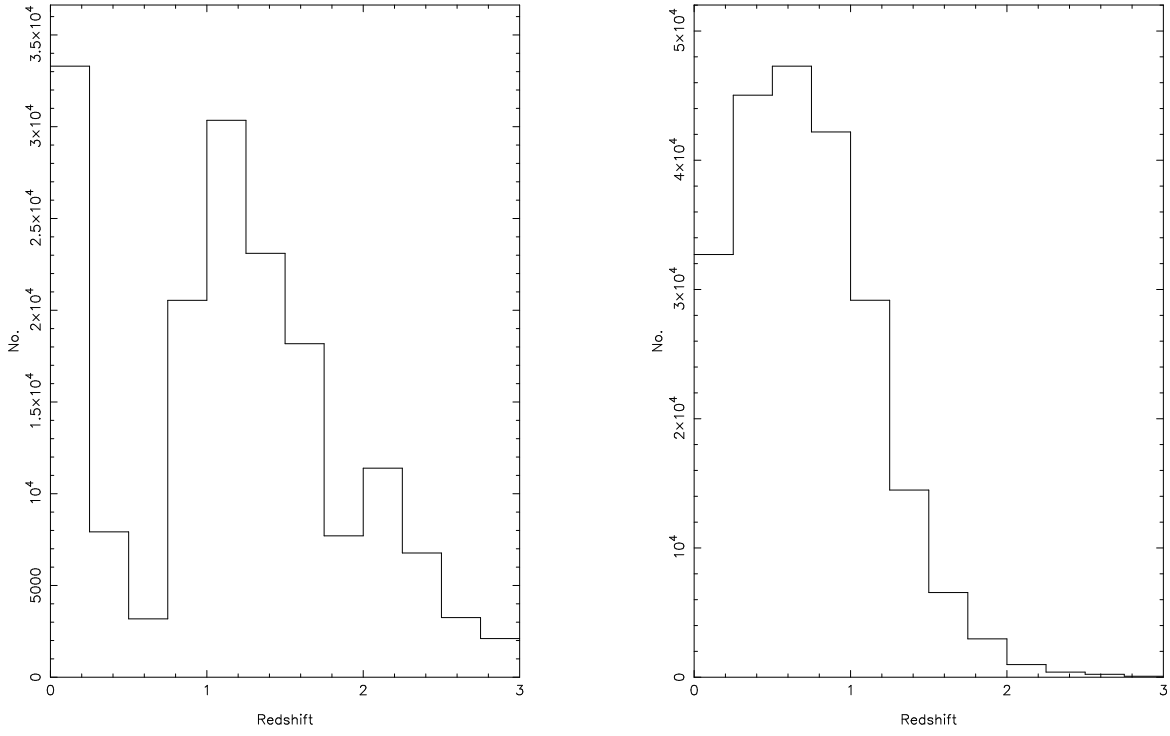


FIG. 3C.— Same as in (a) except at $250 \mu\text{m}$.

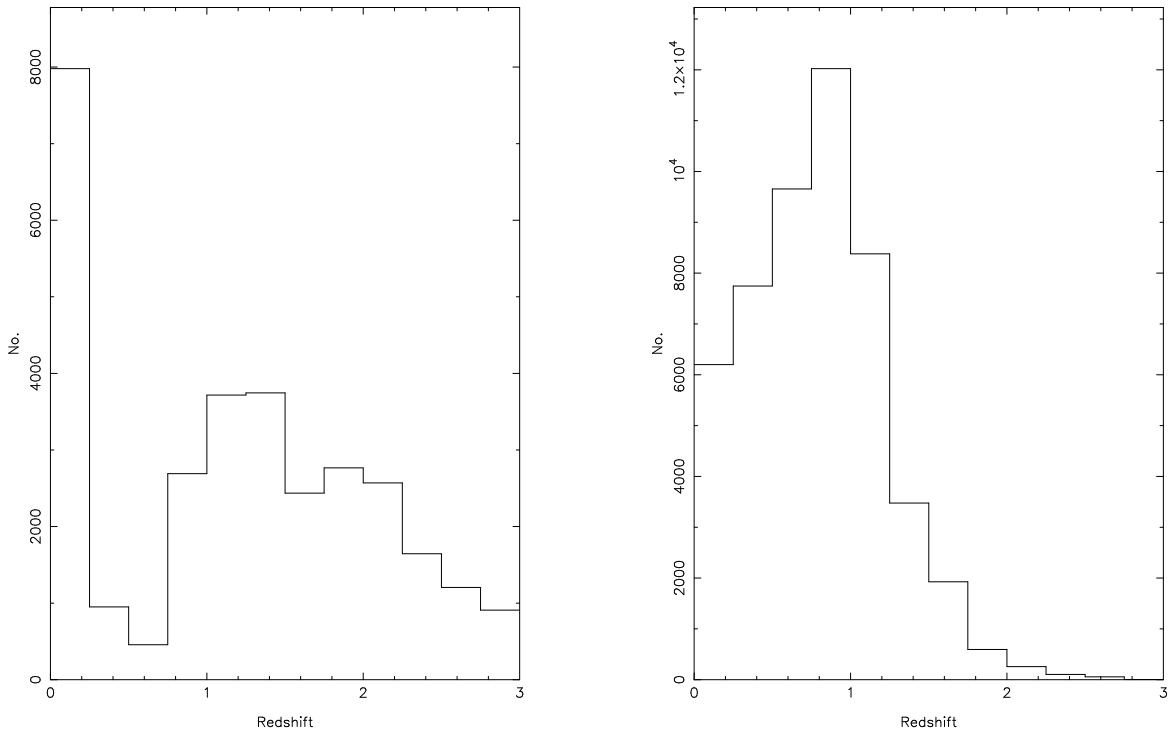
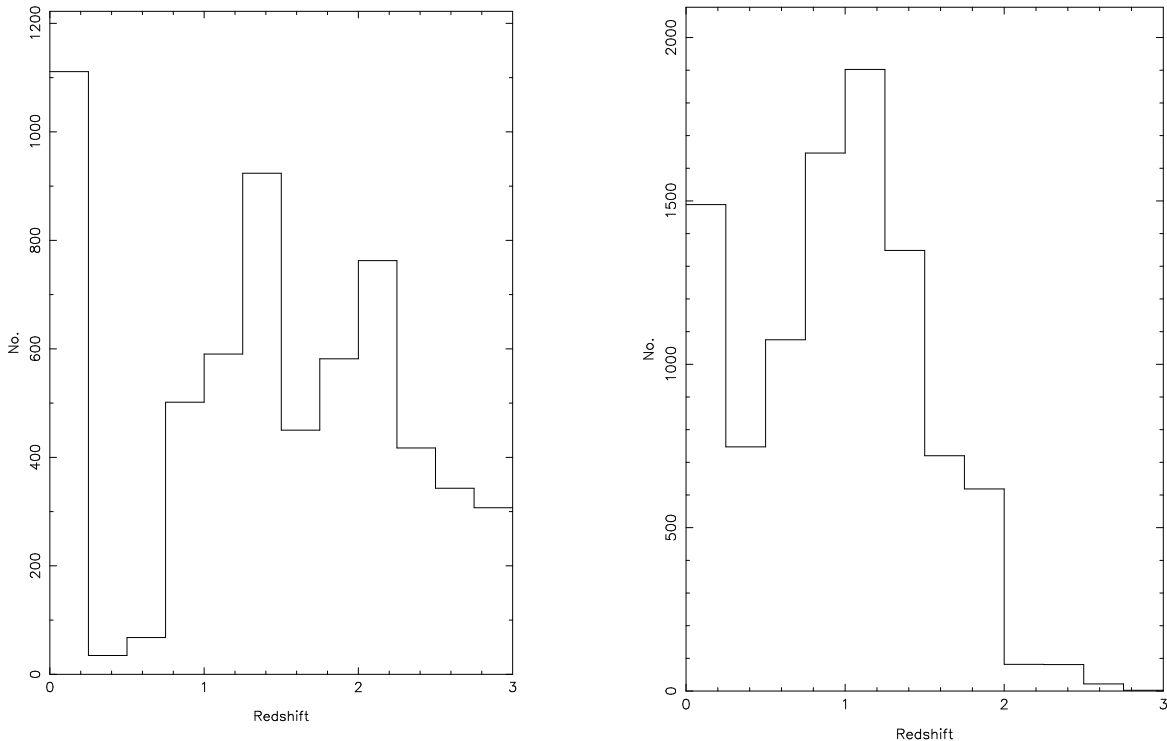


FIG. 3D.— Same as in (d) except at $350 \mu\text{m}$.

FIG. 3E.— Same as in (e) except at 500 μm .

empirical spectral energy distributions that extend from the far-infrared to submillimetre waveband. More sophisticated attempts to use the SLUGS data to predict the local luminosity function suggest that the simple method we present here leads to an underestimate of the local luminosity function (Vlahakis et al. 2005). However, the local submillimetre luminosity function is sufficiently uncertain that we are not too concerned about this—determining the luminosity function is one of the goals of the H-ATLAS—and the simple modelling method we present below has the advantage that it is possible to make predictions for the optical, radio and other properties of the galaxies we will detect with H-ATLAS.

We can use the SLUGS sample to predict the source counts in any submillimetre waveband in a straightforward way. Let us, for example, predict the number of sources in the SPIRE 250 μm band. If we assume ‘number-density evolution’, in which the number of sources of a given luminosity changes with redshift, the number of sources above a given 250 μm flux density is

$$N(> S_{250\mu\text{m}}) = \sum_{j=1}^{104} \int_0^{z(L_j, S_{250\mu\text{m}})} \frac{E(z)}{V_j} dV \quad (1)$$

in which V_j is the comoving volume in which the j 'th SLUGS source could have been detected in the original survey from which it was selected and $E(z)$ is the ratio of the comoving number-density of sources of a given luminosity at a redshift z to the number at zero redshift. The upper limit of the integral is the maximum redshift at which the j 'th source could be placed and just be detected above the 250- μm flux limit. L_j is the luminosity of the j 'th SLUGS source, which can be estimated

at the appropriate rest-frame wavelength at each redshift (for the observed wavelength of 250 μm) from the two-component dust model. In the specific case of the submillimetre waveband, we can use the two-component dust model (Dunne & Eales 2001) to estimate the luminosity at any wavelength. If we assume that rather than density-evolution we have luminosity evolution, in which the number of galaxies stays the same but their luminosities evolve, the equation becomes:

$$N(> S_{250\mu\text{m}}) = \sum_{j=1}^{104} \int_0^{z(L_j, S_{250\mu\text{m}})} \frac{1}{V_j} dV \quad (2)$$

In this case, all the information about cosmic evolution is included in the upper limit because

$$L_j(z) = E(z)L_j(0) \quad (3)$$

in which $E(z)$ is the ratio of the luminosity of a galaxy at redshift z to the luminosity of the galaxy at zero redshift. These equations can be modified in a straightforward way to estimate the source counts at any submillimetre wavelength and also the cosmic background radiation.

In practice, we have used the simple luminosity-evolution model from Rowan-Robinson (2001), in which the rest-frame monochromatic luminosity over the entire far-IR/submillimetre waveband is assumed to evolve in the following way:

$$L(t) = L(t_0) \left(\frac{t}{t_0} \right)^P e^{Q(1 - \frac{t}{t_0})} \quad (4)$$

TABLE 2
PREDICTIONS

Wavelength/redshift range	SLUGS	Lagache
110 μm , total	76944	65973
110 μm , $z < 0.1$	15489	7267
110 μm , $z < 0.3$	39695	18502
170 μm , total	68740	56351
170 μm , $z < 0.1$	10088	7049
170 μm , $z < 0.3$	26761	17883
250 μm , total	222061	170783
250 μm , $z < 0.1$	12500	13321
250 μm , $z < 0.3$	40073	34887
350 μm , total	50422	32636
350 μm , $z < 0.1$	2967	3192
350 μm , $z < 0.3$	7389	8170
500 μm , total	9734	6998
500 μm , $z < 0.1$	856	444
500 μm , $z < 0.3$	1714	1118

NOTE. — Reading from the left, the columns are: the wavelength and the redshift range ('total' means all redshifts); the prediction of the model based on the SCUBA Local Universe and Galaxy Survey (see text for details); the prediction of the Lagache model (Lagache et al. 2003; Lagache et al. 2004)

in which t is the time from the big bang and t_0 is the

time at the current epoch. P and Q are parameters of the model, and we found that $P = 3$ and $Q = 9$ produced acceptable fits to the spectral shape and intensity of the cosmic background radiation (Fixsen et al. 1998) and to the SCUBA 850 μm and Spitzer 70 μm source counts (Coppin et al. 2006, Frayer et al. 2006a,b).

Table 2 shows the total number of sources that this model and the models of Lagache et al. (2003,2004) predict should be detected by H-ATLAS, including the number at $z < 0.1$ and at $z < 0.3$. Figure 3 shows the redshift distributions predicted by the two models. The numbers of sources predicted by the models at the five wavelengths agree fairly well, although there are large differences between the predicted redshift distributions. This difference is not surprising because the observational data used to constrain the models consists almost entirely of number counts, which inform us about the numbers of sources in slices of the luminosity-redshift plane but nothing about the distribution of redshifts within each slice. Both sets of models do agree, however, in predicting that the H-ATLAS will detect a large number of sources in the relatively nearby Universe ($z < 0.3$).

The advantage of the models based on SLUGS is that it is possible to predict the properties of the H-ATLAS sources in any waveband in which the spectral energy distributions (SED) of the SLUGS galaxies have been measured. For example, the number of H-ATLAS galaxies that are predicted to have B-band optical magnitudes in the range $B_1 < B < B_2$ is given by

$$N(B_1 < B < B_2) = \sum_{j=1}^{104} \int_{z_{\min}(B_1, B_2, S_{250\mu\text{m}}, L_j)}^{z_{\max}(B_1, B_2, S_{250\mu\text{m}}, L_j)} \frac{1}{V_j} dV \quad (5)$$

in which the limits of the integral are the maximum and minimum redshifts at which the j 'th galaxy would

fall both within the optical limits and above the 250- μm limit. In calculating these limits, we have assumed that the far-IR/submillimetre luminosity of the SLUGS galaxy is evolving with cosmic time in the way given by equation 4 but that its luminosity in the other waveband is not evolving. This assumption is almost certainly not correct, but given our lack of knowledge of the cosmic evolution in most wavebands it seems the safest (and simplest) one to make. It is also a conservative assumption, in the sense that the model probably underestimates how bright the H-ATLAS sources will be in the other wavebands. The SED of each galaxy is necessary to relate the flux at the observed wavelength—in this case the B-band—to the luminosity of the galaxy at the wavelength at which the radiation was emitted. Similar equations can be written for any waveband.

Figures 4-8 show the predictions for the H-ATLAS galaxies in five bands. The panel on the left-hand side shows the prediction for all the H-ATLAS galaxies and the one on the right for those galaxies at $z < 0.3$.

Figures 4 and 5 show the predictions for the optical B and r bands. Several major redshift surveys have been based on catalogues defined in these bands and in §4 we use these predictions to estimate the fraction of the H-ATLAS galaxies that will already have spectroscopic redshifts. In making the predictions for the B band, we have used the B-band photometry that exists in the NASA Extragalactic Database (NED) for most of the SLUGS galaxies, and we made the assumption that all the SLUGS galaxies have an SED typical of an Sbc galaxy (Coleman et al. 1980). Note that although the assumption of a single optical SED for all H-ATLAS galaxies is a crude one, it should introduce little error at low redshift, where the observed and rest frames are very close in wavelength. We have made the r-band predictions using the V-band photometry, which exists in NED for 75% of the SLUGS galaxies, with a small correction to the r-band using the colour transformations in Jester et al. (2005).

Figure 6 shows the predictions for the K-band. We have used the K-band photometry in NED that exists for almost all the SLUGS galaxies (mostly from 2MASS) and again assumed a standard Sbc SED.

Figure 7 shows the predicted 1.4-GHz continuum radio fluxes of the H-ATLAS galaxies. We have made the prediction for the continuum radio fluxes using the 1.4-GHz flux measurements that exist for almost all the SLUGS galaxies plus the assumption that all the SLUGS galaxies have a power-law radio continuum ($S \propto \nu^{-\alpha}$) with $\alpha = 0.7$. In this case, it seems quite likely that the assumption of no evolution in the radio waveband is incorrect because of the strong correlation between the far-infrared/submillimetre and radio emission from star-forming galaxies both at low and high redshift (Helou et al. 1986; Ibar et al. 2009). We have therefore assumed that radio luminosity also evolves in the way given by equation 4.

Figure 8 shows the prediction for the HI line fluxes of the H-ATLAS galaxies. We used the HI line fluxes for the SLUGS galaxies given in NED. We have assumed that the amount of atomic hydrogen in a galaxy does not evolve, which may mean that the predicted HI line fluxes of the H-ATLAS galaxies are underestimated.

The figures show that, in contrast to the sources de-

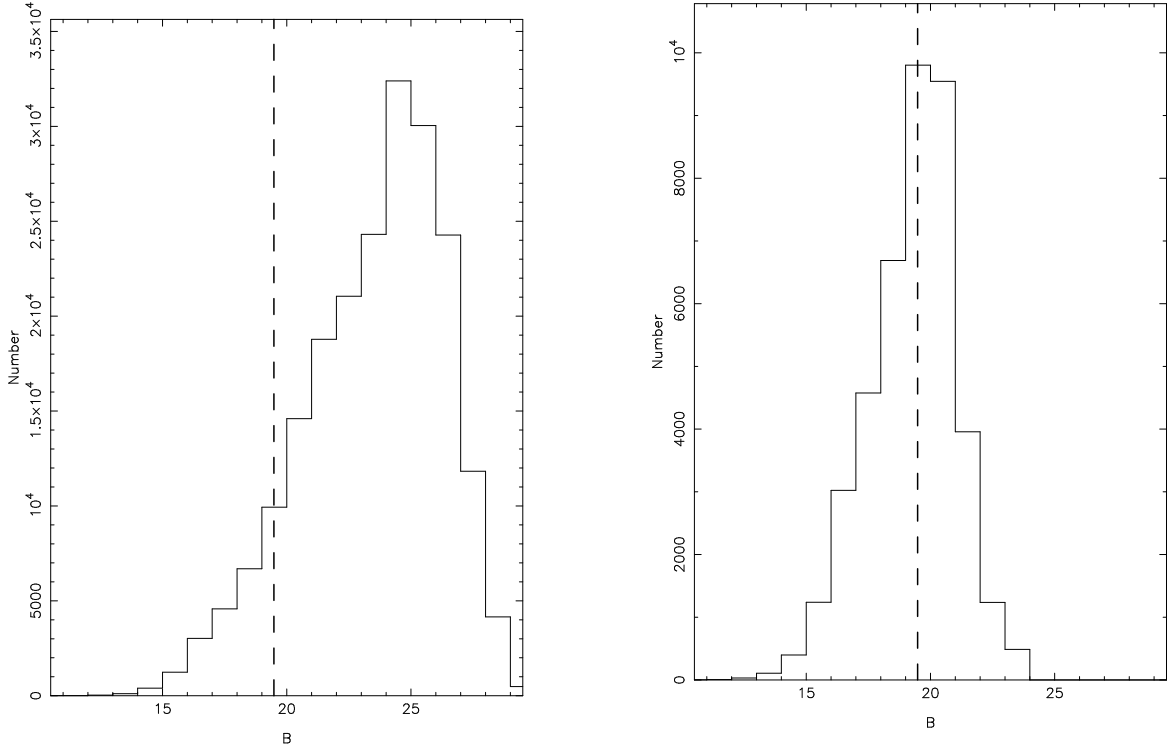


FIG. 4.— The histogram of B-band optical magnitude predicted for the H-ATLAS galaxies using the method described in the text. On the left is the prediction for all the galaxies and on the right is the prediction for those at $z < 0.3$. The vertical dashed line shows the magnitude limit of the 2dF Galaxy Redshift Survey.

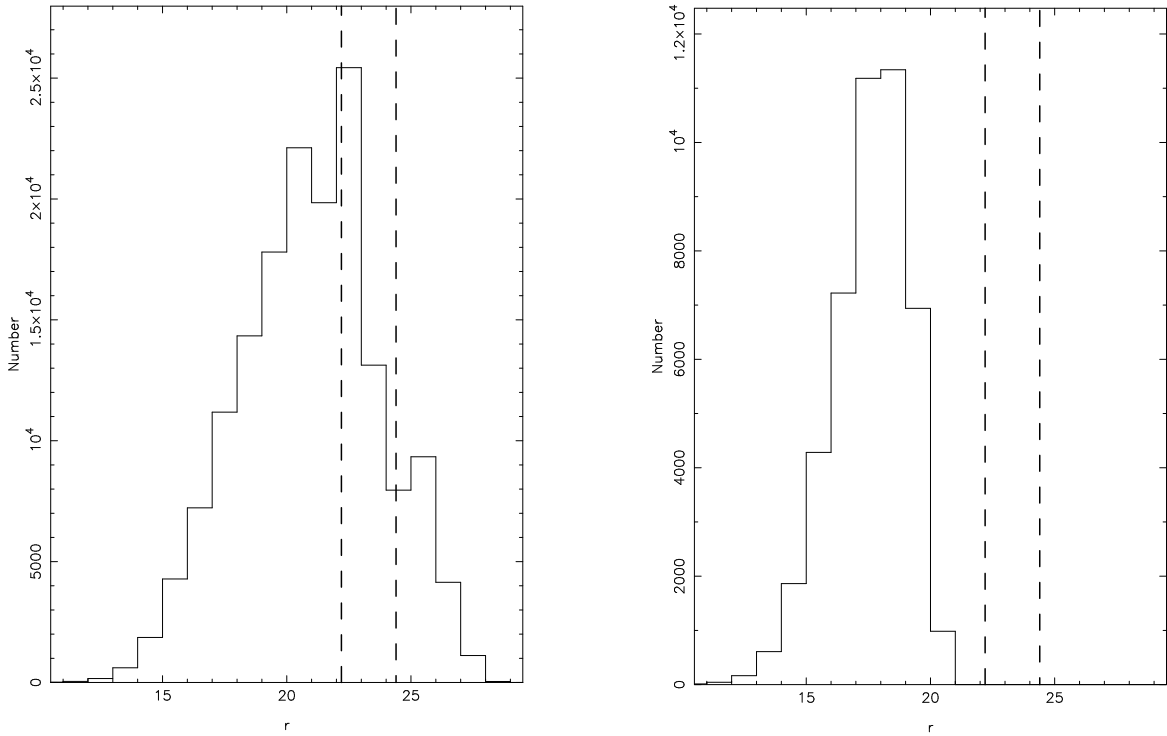


FIG. 5.— The histogram of r-band optical magnitude predicted for the H-ATLAS galaxies using the method described in the text. On the left is the prediction for all the galaxies and on the right is the prediction for those at $z < 0.3$. The vertical dashed line on the left shows the limiting magnitude of the imaging part of the Sloan Digital Sky Survey; the one on the right shows the approximate limit that will be reached by the ESO public survey KIDS.

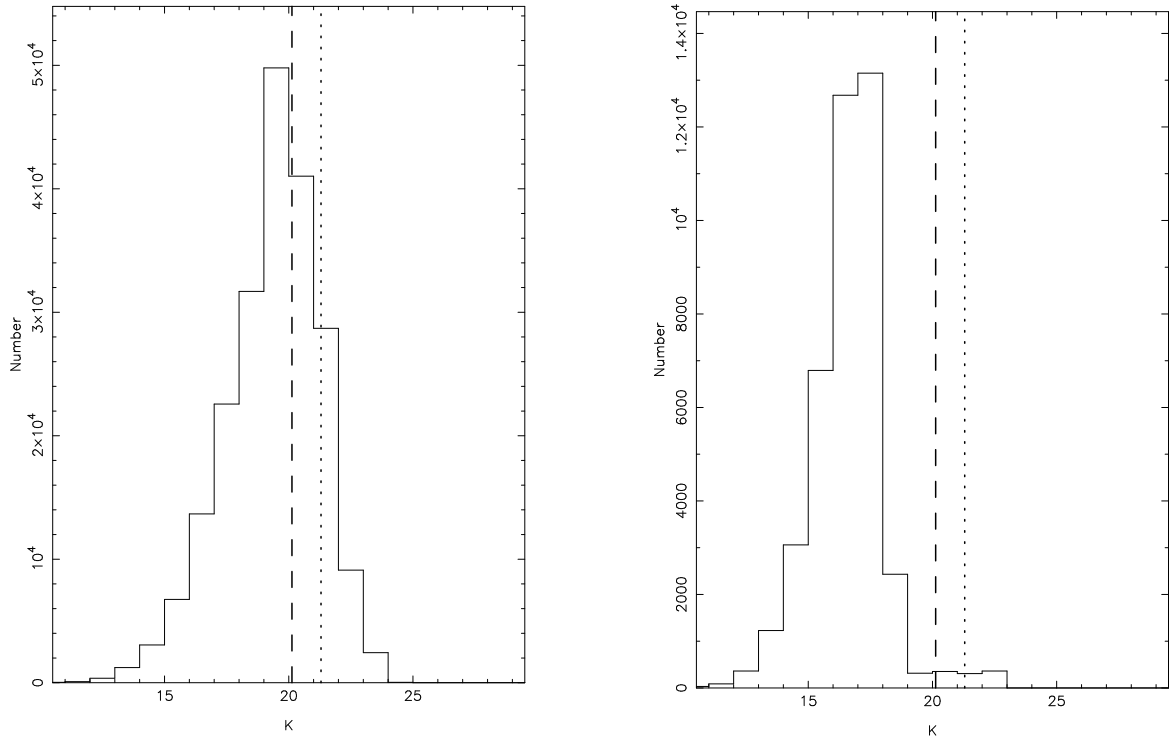


FIG. 6.— The histogram of K-band optical magnitude predicted for the H-ATLAS galaxies using the method described in the text. On the left is the prediction for all the galaxies and on the right is the prediction for those at $z < 0.3$. The left-hand vertical dashed line shows the limiting magnitude of the Large Area Survey that is part of the UKIRT Infrared Deep Sky Survey (Warren et al. 2007). The right-hand vertical line shows the limiting magnitude of the ESO public survey, VIKING.

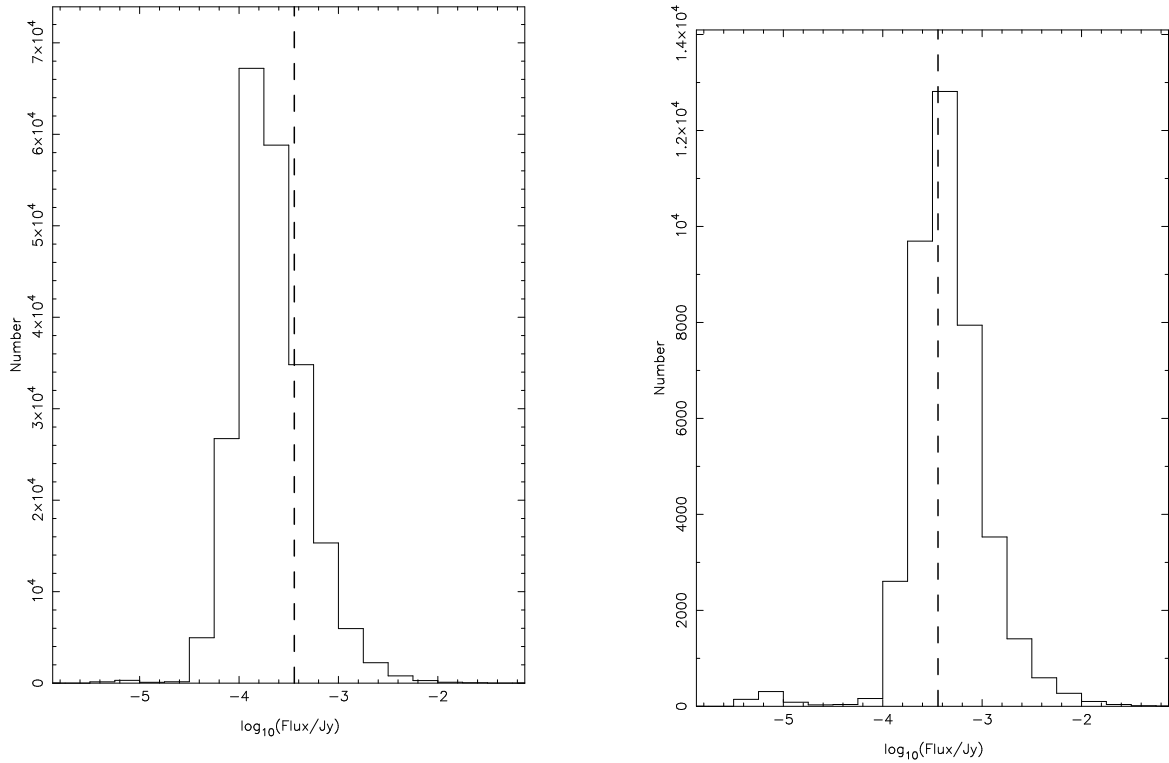


FIG. 7.— Histogram of the 1.4-GHz radio fluxes predicted for the H-ATLAS galaxies using the method described in the text. On the left is the prediction for all the galaxies and on the right is the prediction for those at $z < 0.3$. The vertical dashed line shows the approximate 5σ limit of the radio survey we are carrying out with the GMRT, translated to 1.4 GHz using the assumption of a power-law radio spectrum ($S \propto \nu^{-\alpha}$) with $\alpha = 0.7$ (§4.3).

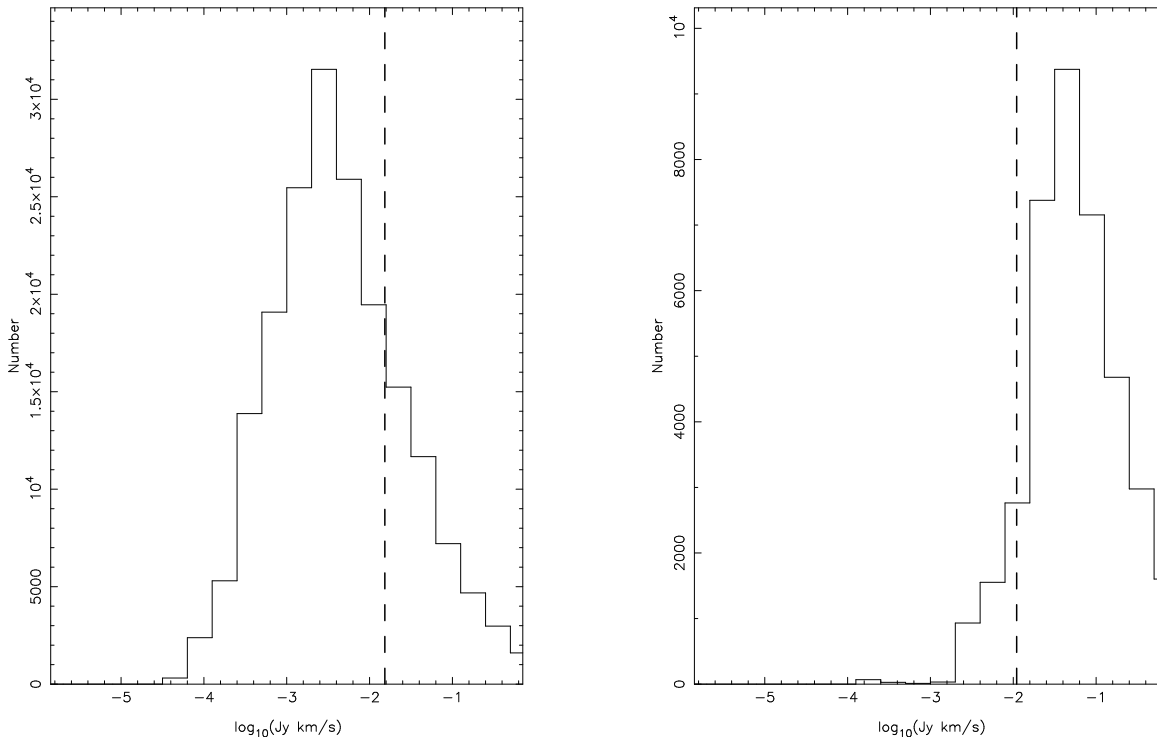


FIG. 8.— Histogram of the 21-cm line fluxes predicted for the H-ATLAS galaxies using the method described in the text. On the left is the prediction for all the galaxies and on the right is the prediction for those at $z < 0.3$. The vertical dashed line shows the approximate 5σ limit of the HI survey described in §4.3.

tected in the SCUBA surveys at $850 \mu\text{m}$, it should be fairly easy to follow-up the H-ATLAS sources with observations in other wavebands.

4. MULTI-WAVELENGTH DATA

We selected our fields partly because of the low ‘cirrus emission’ from dust in our own galaxy (Fig. 2) but mainly because the complementary multi-wavelength data is better than for any field of similar size. We describe here the multi-wavelength datasets, both ones that exist now and ones that are likely to soon exist.

4.1. Spectroscopy

There have been three major recent redshift surveys: the Sloan Digital Sky Survey (SDSS - York et al. 2000); the 2dF Galaxy Redshift Survey (2dFGRS - Colless et al. 2001) and the Galaxy And Mass Assembly Survey (GAMA - Baldry et al. 2009, Driver et al. 2009). The GAMA survey is still underway. All of the H-ATLAS fields are covered by one or more of these surveys. We have used the models from the last section to predict the number of H-ATLAS sources that will already have redshifts from one of these surveys. In making these predictions, we have made the assumptions that (a) the 2dFGRS measured redshifts for 93% of the galaxies with $B < 19.6$ (Colless et al. 2001)⁵⁴, (b) that the SDSS measured redshifts for 94% of galaxies with $r < 17.77$ (Strauss et al. 2002) and (c) that GAMA will measure redshifts for all galaxies with $r < 19.4$ (Driver et al. 2009). Table 3 lists the predicted numbers

⁵⁴ We have made the transformation from the b_j magnitude system using the relationship $b_j = B - 0.28(B - V)$ given in Maddox et al. (1990).

of sources which will already have spectroscopic redshifts in the different fields. The table shows that $\sim 2 \times 10^4$ H-ATLAS galaxies are likely to already have spectroscopic redshifts, and that the percentage of H-ATLAS galaxies at $z < 0.1$ with spectroscopic redshifts is likely to be very high. All three surveys, of course, contain far more information about the galaxies than only the redshifts, such as measurements of line ratios, line equivalent widths, kinematics etc.

4.2. Imaging from the ultraviolet to the near infrared

At ultraviolet wavelengths, approximately half the total survey area has been observed with GALEX. This has mostly been part of the GALEX Medium Imaging Survey (MIS), which has an exposure time of 1500s and a limiting AB magnitude of $\simeq 23$. We and the GAMA team have been awarded time for a proposal to complete the GALEX coverage of the GAMA fields to the MIS depth (P.I. Tuffs).

In the optical waveband, the GAMA fields and the NGP field have been surveyed in five passbands by the Sloan Digital Sky Survey. The limiting magnitude of the r-band imaging is shown in Figure 5. As yet, the SGP field has only been surveyed with the UK Schmidt Telescope using photographic plates. In the next three years, the H-ATLAS fields should be covered by three new optical surveys. The GAMA and SGP fields will be observed in four passbands as part of the Kilo Degree Survey (KIDS), an ESO public survey that will be carried out with the VLT Survey Telescope (VST). The sensitivity limits of KIDS will be about 2 magnitudes fainter than the SDSS limits. The NGP and GAMA fields will be observed in five bands by Pan-STARRS1 and the SGP and GAMA fields will be observed in six

TABLE 3
REDSHIFT SURVEYS

H-ATLAS field	Datasets	No. at $z < 0.1$	No. at $z < 0.3$
NGP	SDSS	3366 (2895)	10865 (4563)
GAMA	GAMA,SDSS,2dFGRS	3366 (3366)	10865 (9456)
SGP	2dFGRS	5610 (4993)	18106 (8148)
All fields	...	12342 (11254)	39833 (22167)

NOTE. — Reading from the left, the columns are: the H-ATLAS fields; the redshifts surveys covering this field; the predicted number of sources at $z < 0.1$ in this field with the predicted number with spectroscopic redshifts in brackets; the predicted number of sources at $z < 0.3$ in this field with the predicted number with spectroscopic redshifts in brackets

bands by SkyMapper (Keller et al. 2007). The approximate 5σ limits for all the optical surveys are given in Table 4. A little further off in time, the SGP field will be observed as part of the Dark Energy Survey.

In the near infrared, the GAMA and NGP fields are being surveyed in four passbands as part of the Large Area Survey (LAS), a legacy survey being carried out as part of the UKIRT Infrared Deep Sky Survey (Warren et al. 2007). The GAMA and SGP fields will soon be observed in five passbands as part of the VISTA Kilo-Degree Infrared Galaxy Survey in the Infrared (VIKING), an ESO public survey that is currently being carried out with the Visible and Infrared Telescope for Astronomy (VISTA). The approximate limits of both surveys are given in Table 4 and shown in Figure 6.

4.3. Radio Surveys - continuum and HI

The H-ATLAS fields have been surveyed at 1.4 GHz as part of the NRAO VLA Sky Survey. This survey is not sensitive enough, however, to detect a significant percentage of the H-ATLAS sources. We are therefore currently completing a radio survey (P.I. Jarvis) of the GAMA fields at 325 MHz with the Giant Metre-wave Radio Telescope (GMRT), which will reach an approximate 5σ sensitivity of 1 mJy. The limit of this survey is shown in Figure 7. The NGP field is also high on the list of targets for an early survey with the Low Frequency Array for Astronomy (LOFAR).

There is currently no HI survey of any of the H-ATLAS fields that could yield HI measurements of a significant fraction of the H-ATLAS sources. However, the SGP and GAMA fields are natural targets for the new southern radiotelescopes that are being built as prototypes for the Square Kilometre Array (and for the SKA itself, of course). We have designed a potential HI survey of the SGP field using the parameters given for the Australian Square Kilometre Pathfinder Array (ASKAP) by Johnston et al. (2007). We estimate that in one month of observing time it should be possible to carry out a survey of the SGP sensitive to galaxies out to $z \simeq 1$ with an approximate sensitivity to HI flux of $\simeq 10^{-2}$ Jy km s $^{-1}$ (Fig. 8).

4.4. Planck and other telescopes

The Planck Surveyor is surveying the whole sky in nine passbands, two of which (350 and 550 μm) are the nearly the same as those that will be used in H-ATLAS. The size (full-width-half-maximum) of the Planck beam is $\simeq 10$ times greater than that of H-ATLAS at the same fre-

quency, although the sensitivity in surface brightness is fairly similar. Therefore, in the common area of the sky (one eightieth of the whole sky), the two surveys will be complementary, with the H-ATLAS providing high-resolution observations of the sources that will be detected by Planck.

The SGP field may also be observed by the South Pole Telescope, a telescope designed to look for high-redshift clusters using the Sunyaev-Zeldovich effect.

5. THE H-ATLAS SCIENCE PROGRAMME

In this section we describe the six major science programmes planned by the H-ATLAS team. We note that these programmes represent only a limited subset of the scientific projects that will be ultimately possible with the H-ATLAS for two reasons. First, many other projects will become possible as the surveys of the H-ATLAS fields at other wavelengths (§4) are gradually completed. Second, since the wavelength range from 200 to 500 μm is virtually unexplored and since the H-ATLAS will cover one eighth of the sky in this waveband, it is possible that there will be some unanticipated discoveries.

5.1. The Local Universe

Our models (§4) predict that the H-ATLAS will detect $\simeq 40,000$ galaxies in the relatively nearby Universe ($z < 0.3$). Almost all the galaxies detected at $z < 0.1$ and approximately half the galaxies detected at $z < 0.3$ should already have spectroscopic redshifts. Most of these galaxies will be unresolved by the H-ATLAS beams. There are $\simeq 120$ clusters of Abell richness class 1 or greater, including the Coma Cluster, in our fields.

Apart from providing the spectroscopic redshifts necessary to calculate the intrinsic properties of many of the sources (luminosities, dust masses etc.), the complementary data will be helpful in other ways. Three are particularly important. First, the redshift surveys will allow us to determine the position within the cosmic web of each Herschel galaxy and to measure the density of the galaxy’s environment (exactly how to do this best is debateable—e.g. Balogh et al. 2004). Second, the existence of catalogues at other wavelengths means that the H-ATLAS will contain more information than the individual source detections. By coadding (‘stacking’) the Herschel emission at the positions of objects in different classes, we can study the dust and dust-obscured star formation in objects that would be too faint to detect individually (Dole et al. 2006; Dye et al. 2007b). An important example is elliptical galaxies (§1). Third, we

TABLE 4
OPTICAL AND NEAR INFRARED DATA

H-ATLAS field	Datasets	u	v	g	r	i	z	Z	y	Y	J	H	K
NGP	SDSS	22.0	...	22.2	22.2	21.3	20.5
NGP	Pan-STARRS1 ^a	24.1	23.5	23.4	22.4	...	21.2
NGP	LAS	20.87	20.55	20.28	20.13
GAMA	SDSS	22.0	...	22.2	22.2	21.3	20.5
GAMA	KIDS	24.0	...	24.6	24.4	23.4
GAMA	Pan-STARRS1 ^a	24.1	23.5	23.4	22.4	...	21.2
GAMA	SkyMapper ^b	22.9	22.7	22.9	22.6	22.0	21.5
GAMA	LAS	20.87	20.55	20.28	20.13
GAMA	VIKING	23.1	...	22.4	22.2	21.6	21.3
SGP	KIDS	24.0	...	24.6	24.4	23.4
SGP	SkyMapper ^b	22.9	22.7	22.9	22.6	22.0	21.5
SGP	VIKING	23.1	...	22.4	22.2	21.6	21.3

NOTE. — Reading from the left, the columns are: the H-ATLAS field; the optical or near-IR survey; the quoted sensitivity limits in AB magnitudes (These are 5σ limits for point sources, except in the case of the SDSS in which the limits represent the 95% detection repeatability for point sources).

^a The limits are for the planned three-year survey with Pan-STARRS1.

^b The limits are for the planned six-epoch survey by SkyMapper.

will be able to answer the question of what fraction of the optical light from a galaxy is obscured by dust. Optical astronomers have struggled with this issue for 50 years (Holmberg 1958; Davies and Burstein 1995) with limited success, largely because optical galaxy catalogues have large selection effects caused by dust. The implications for extragalactic astronomy are potentially large, with a recent study concluding that the optical luminosity function is significantly altered by dust extinction and that even bulges suffer as much as 2 mag of extinction at certain inclinations (Driver et al. 2007). The ultraviolet, optical and near-infrared data that exist for some of the fields (§4) will allow us to address this issue by the simple energy-balance technique of comparing the total dust emission to the total unobscured starlight. The only assumption in this technique is that the absorption by the dust is isotropic. This is almost certainly untrue but by averaging over many objects we can largely eliminate the effects of anisotropy (Driver et al. 2008).

We give the following four projects as examples:

- We will make the first accurate estimate of the local submillimetre luminosity and dust-mass functions down to dust masses of $\sim 10^{4.5} M_{\odot}$ (Fig. 9). As we will have Herschel measurements for $\simeq 10,000$ galaxies at $z < 0.1$, we will be able to compare the luminosity and dust-mass functions for different classes of galaxy (e.g. different Hubble types, high and low environmental density etc.). We will also be able to extend the study of the luminosity and dust-mass functions to higher dimensions, for example by examining how the space density of galaxies depends on both dust mass and stellar mass.
- Using the results from the redshift surveys, we will investigate how the dust-obscured star formation depends on the local and large-scale environment. This complements previous optical studies (Balogh et al. 2004; Kauffmann et al. 2004), because our observations will be much more sensitive to starbursts, which may well have a different environmental dependence from quiescent star for-

mation.

- We will investigate how the dust content of the Universe and dust-obscured star formation has changed during the last three billion years. This will finally follow up an important discovery from IRAS that there is strong evolution in the luminosity function at a surprisingly low redshift (Saunders et al. 1990), a phenomenon which also may have been seen in the SDSS (Loveday et al. 2004).
- One of the strongest correlations in astronomy is that between the far-infrared and nonthermal radio emission of galaxies (Helou et al. 1986; Ibar et al. 2009). A widely-accepted explanation is that both the far-infrared emission and the radio emission are ultimately caused by young stars, with the far-infrared emission being from the dust heated by young stars and the radio emission being nonthermal emission from the relativistic electrons generated in the supernova remnants produced when the stars reach the end of their lives. Nevertheless, many of the properties of this relationship are hard to explain, in particular the approximate unity slope when the two quantities are plotted on logarithmic axes (Vlahakis et al. 2007). By investigating this relationship as a function of environment, redshift, star-formation activity and other properties, we will try to understand better its fundamental cause.

5.2. Planck Point Sources and Diffuse Emission

The Planck High-Frequency Instrument (HFI) will survey the whole sky in six bands (3, 2.1, 1.4, 0.85, 0.55, 0.35 mm), the first survey of the whole sky at these wavelengths. Apart from its measurements of the primordial cosmic background radiation (CMB), the HFI will detect extended foreground emission, such as dust in the Galaxy, and it is also likely to detect many point sources (de Zotti et al. 2005), including nonthermal radio sources, thermal dust emission from nearby galaxies and Sunyaev-Zeldovich (SZ) sources associated with

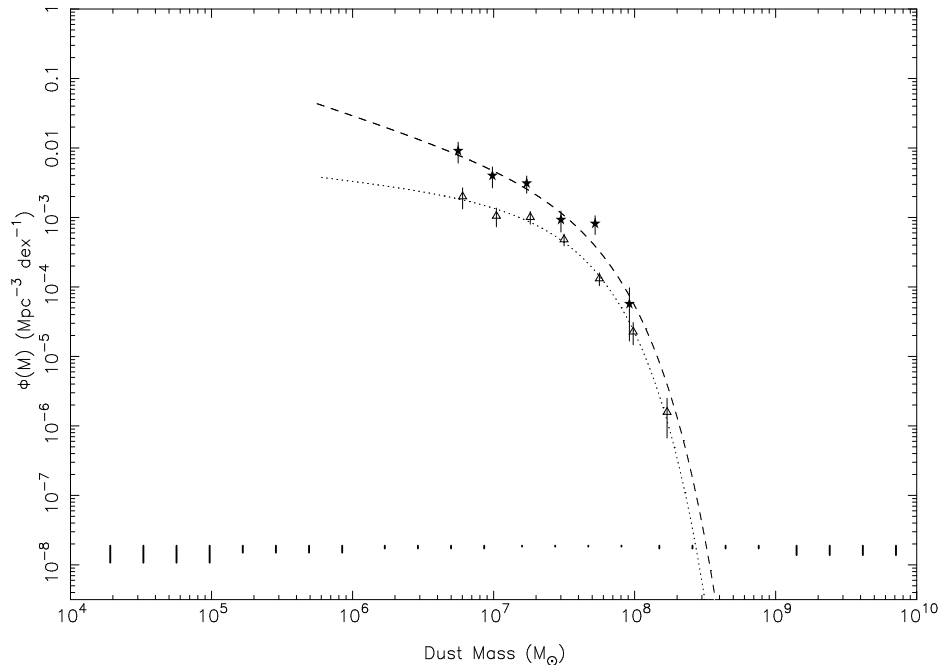


FIG. 9.— The triangles and stars show estimates of the dust-mass function (the space-density of galaxies as a function of dust mass) from Vlahakis, Dunne and Eales (2005). The vertical lines along the bottom show our estimates, on the assumption of Poisson statistics, of the $\pm 1\sigma$ errors on the estimate of the dust-mass function from the H-ATLAS.

distant clusters, the consequence of the scattering of the CMB radiation by the electrons in the intracluster medium.

The SZ sources detected by Planck are potentially of great importance for cosmologists, because the number-density of clusters as a function of redshift depends critically on the cosmological model (Bartelmann 2001; Bartelmann and White 2002). It might also be possible, because the spectral shape of the SZ effect depends on the peculiar motion of the cluster, to measure bulk flows in the universe (Kashlinsky and Atrio-Barandela 2000), which is another critical test of the cosmological paradigm. A major problem, however, is the contamination of the SZ effect by thermal emission from dusty galaxies within the large (5-10 arcmin) Planck beam, because there is evidence that even at moderate redshift the combined emission from dust in cluster galaxies is comparable to the SZ effect in the 0.85-mm band, and much greater in the two shorter wavelength bands (Zemcov 2007). There is zero SZ effect at 1.4 mm, which leaves only the two long-wavelength bands with little contribution from dusty galaxies, but as these also have the worst angular resolution there is the additional problem of confusion with nonthermal radio sources.

The H-ATLAS will survey one eightieth of the sky in the two Planck bands with the highest frequencies, but with much better resolution. The sensitivity to extended regions of low surface brightness of the two surveys is likely to be similar. The combination of the two surveys will make possible several joint projects:

- The effects of confusion on the Planck point source catalogue are likely to be large, particularly in the highest frequency channels. These include Eddington bias (Eddington 1940), which can lead to both overestimates of the fluxes of the sources and spurious detections, and a large and uncertain effect

on the positions of the sources. The H-ATLAS will provide a sample of sources with accurately known positions and fluxes, which can then be checked against the Planck point-source catalogue for the same area of sky for the two highest frequency channels. This comparison will provide an estimate of the correction factor for the Planck fluxes, an estimate of the fraction of the Planck sources that are spurious, and measurements of the positional errors of the Planck sources.

- Some of the Planck science goals, such as the detection of the anisotropies in the cosmic infrared background (Lagache et al. 2003; Lagache et al. 2004), require the successful removal of galactic cirrus emission. The galactic cirrus should be easier to distinguish in the H-ATLAS images because of the better angular resolution, and so we will be able to test the success of the Planck component separation techniques.
- The combination of the high-resolution images provided by H-ATLAS and the spectral energy distributions of the Planck sources should make it possible to determine unambiguously the nature of each source in the overlap region between the two surveys. The detailed information provided by the H-ATLAS for the Planck sources in this region will make it possible to develop better statistical methods based on their spectral energy distributions for determining the nature of the Planck sources in the region not covered by H-ATLAS.
- In the overlap region between the two surveys, the H-ATLAS will make it possible to determine the contribution of dusty galaxies to each SZ source and then subtract these galaxies' emission from the

SZ signal. The detailed information in the overlap region will also provide statistical information about the average level of contamination for the Planck SZ sources not covered by H-ATLAS.

5.3. *The H-ATLAS Lens Sample*

In principle, gravitational lensing is a powerful way of investigating the evolution in the mass profiles of galaxies, a fundamental test of models of structure formation. In practice, it has proved very hard to assemble the necessary large sample of lenses. The most ambitious programme to date searched for lenses among flat-spectrum radio sources but, after high-resolution radio observations, found only 22 lenses out of 16000 radio sources—a success rate of 0.14% (Browne 2003).

Submillimetre surveys are possibly the ideal way to find lenses. At $z \geq 1$, the monochromatic flux density at the long-wavelength end of the submillimetre waveband depends on luminosity but is approximately independent of redshift, a consequence of the characteristic spectral energy distribution of dust in galaxies. A result of this and the strong cosmic evolution in the submillimetre waveband is that sources in submillimetre surveys tend to lie at high redshifts (§1) and are thus likely to have a large optical depth to lensing. Because of the approximate independence of flux and redshift, a bright source in a submillimetre survey must necessarily have a high luminosity unless it is at $z \leq 1$. Above a critical flux density, the luminosities of any sources beyond this redshift must lie above the luminosity at which the luminosity function declines steeply—and so any sources above this flux density are highly likely to be lensed systems.

The model in Figure 10, for example, predicts that at $S_{500\mu\text{m}} > 100$ mJy the sources should be a mixture of lensed high-redshift galaxies, nearby galaxies and flat-spectrum radio sources (Negrello et al. 2007). Since the latter two categories would be easy to remove (by using the submillimetre flux ratio or the presence of a bright galaxy), the lens yield of such a sample would be close to 100%. These models predict that the H-ATLAS will contain ~ 1500 , 800 and 350 strongly-lensed galaxies at 250, 350 and 500 μm , respectively.

This is the one of the H-ATLAS science programmes for which follow-up observations will be necessary, both to determine whether a bright 500- μm source is indeed a lensed system and to scientifically exploit the H-ATLAS lens sample. Fortunately, a source with $S_{500\mu\text{m}} \sim 100$ mJy would be easy to map; a 30-minute observation with the Submillimetre Array, a one-hour observation with the VLA or a $\simeq 1$ -min observation with ALMA would be enough to confirm a source is a lens and to map the image structure. The prediction that large-area submillimetre surveys are the ideal way to construct large samples of lenses may not be correct, but if it is, there are many possible uses for a large sample of lenses. These include:

- an investigation of the evolution of the profiles of the lenses (probably mostly elliptical galaxies). In principle, it should be possible to use standard techniques (Dye et al. 2007a) to reconstruct separately the structures of the dark-matter halo and baryonic component of each lens.

- a study of the structures of high-redshift dust sources by reconstructing the original (unlensed) structure of the source (Fig. 10). Since our systems are lensed, we will be able to study galaxies well below the Herschel confusion limit (Smail et al. 1997).

5.4. *Active Galactic Nuclei*

The discovery that most nearby galaxies contain a black hole and the mass of the black hole is strongly correlated with the mass of the surrounding spheroid of stars (Magorrian et al. 1998) was possibly one of the most important discoveries in extragalactic astronomy in recent years, because it implies the formation of the stars and the central black hole in a galaxy are connected. Previous submillimetre observations of high-redshift quasars have detected $\simeq 5$ -10% of these objects (Priddey et al. 2003; Beelen et al. 2006), and the spectral energy distributions of the detected quasars imply that most of the submillimetre emission must be coming from a starburst surrounding the active nucleus rather than directly from the nucleus itself. This supports the idea that formation of the stars and the formation of the central black hole in a galaxy are connected.

We will use the H-ATLAS to detect both individual active galactic nuclei that fall in our fields and to carry out statistical analyses of AGN that are too faint to detect individually by coadding (‘stacking’) the Herschel emission at the positions of all the AGN in a given class. Let us consider as an example Type 1 quasars. Figure 11 shows quasars drawn from the Palomar Green (PG) survey and the SDSS as a function of redshift and optical luminosity. Because of the strong correlation between luminosity and redshift in any flux-limited sample, it is crucial to observe more than one sample, so that one can compare quasars with the same optical luminosity at different redshifts and vice versa. The detection rate of PG quasars by IRAS and ISO is $\simeq 80\%$ (Haas et al. 2003). We will use the H-ATLAS to extend the far-IR/submillimetre study of quasars to the more distant SDSS quasars, of which there are $\simeq 10^4$ in the H-ATLAS fields. Using the results of a pilot study with the Spitzer legacy survey SWIRE (Serjeant et al. 2009), we estimate that we will detect $\simeq 440$ quasars at $z < 3$ and $\simeq 210$ quasars at $z > 3$. This is $\simeq 15$ times greater than the number of existing detections of high-redshift quasars. We will investigate the properties of the quasars that are too faint to detect individually by a stacking analysis.

5.5. *Large-Scale Structure*

The H-ATLAS will detect $\sim 200,000$ sources with a median redshift of ~ 1 and will therefore contain a large amount of information about large-scale structure upto a scale of $\simeq 1000$ Mpc at $z \sim 1$. Many large-scale structure projects, such as searches for baryonic oscillations, will only become possible in the future, as the near-IR (VIKING, UKIDSS) and optical (KIDS, Pan-STARRS, the Dark Energy Survey) surveys eventually provide photometric redshift estimates for most of the sources. There are two projects that are possible immediately:

- The H-ATLAS will make possible measurements of the angular correlation function on very large scales. These measurements will make it possible

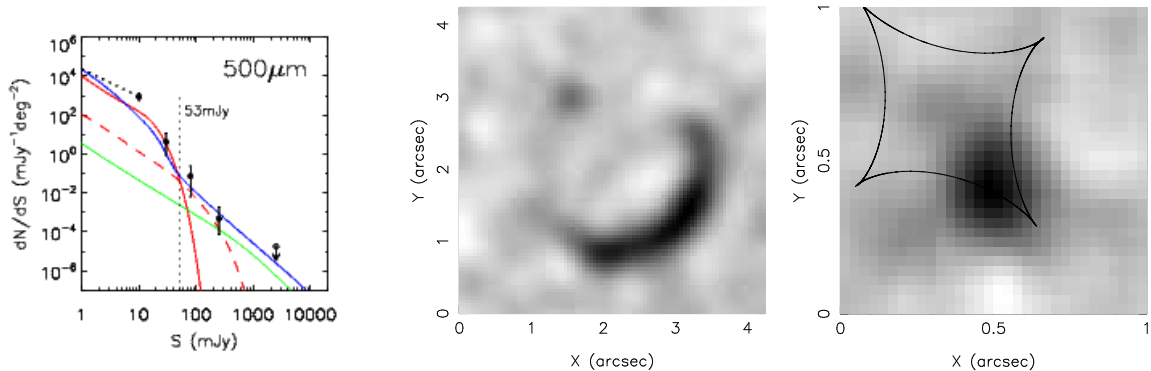


FIG. 10.— The left-hand panel shows the predicted number of sources as a function of $500\ \mu\text{m}$ flux density plotted over the results from BLAST (Negrello et al. 2007). The key to the curves is as follows: red solid—unlensed high- z protospheroids; red dashed—lensed high- z protospheroids; green—blazars; blue—nearby late-type galaxies. The vertical dashed line shows the approximate limit of H-ATLAS at $500\ \mu\text{m}$. The middle panel shows a simulated image of a strongly lensed $100\ \text{mJy}$ $500\ \mu\text{m}$ H-ATLAS source as observed using the Submillimetre Array at $870\ \mu\text{m}$ in extended mode over a 6h track. The panel on the right shows the reconstructed source obtained by applying the reconstruction method of Dye et al. (2007a) to the simulated ring image. The image caustic of the best fit lens model is over-plotted.

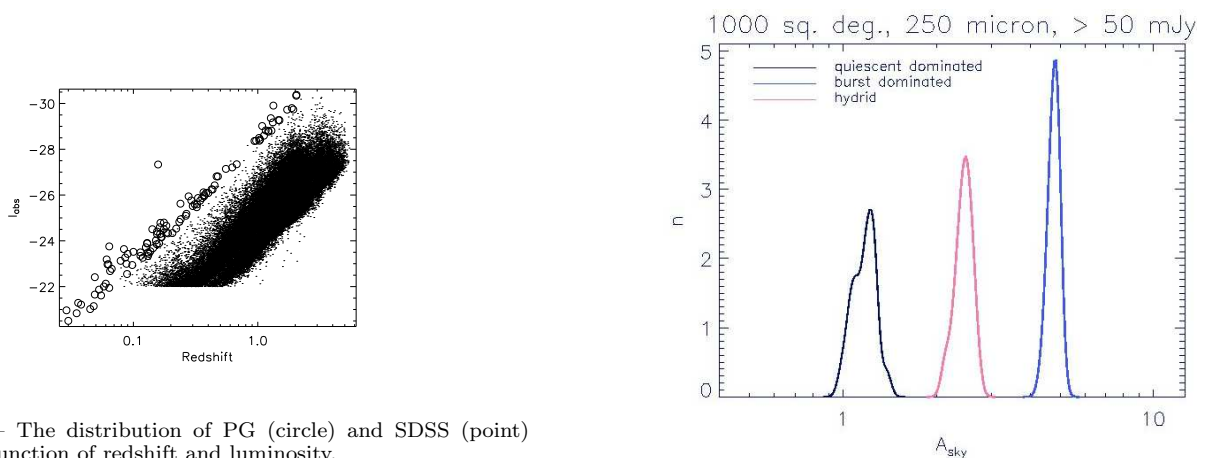


FIG. 11.— The distribution of PG (circle) and SDSS (point) QSOs as a function of redshift and luminosity.

to discriminate between some models of galaxy formation. Figure 12, for example, shows the results of using a Monte-Carlo simulation to predict the amplitude of the angular correlation function of H-ATLAS sources using three alternative models of galaxy formation: the hybrid model from Van Kampen et al. (2005) and two new models (Van Kampen et al. in preparation). The simulation shows that it should be easy to discriminate between these models.

- The individual sources, however, only represent $\simeq 10\%$ of the extragalactic background radiation at the Herschel wavelengths and the unresolved background contains a wealth of further information about the clustering properties of dusty galaxies. A powerful technique to extract further information is to investigate the clustering properties of the intensity distribution on the maps after the high signal-to-noise sources have been removed (Amblard and Cooray 2007; Lagache et al. 2007). The strength of the fluctuations on large angular scales (linear regime) can be used to estimate the average mass of the dark matter halos containing the sources, whereas the strength of the fluctuations on small angular scales (non-linear regime) can be used to estimate the halo occupancy distribution (Amblard and Cooray 2007).

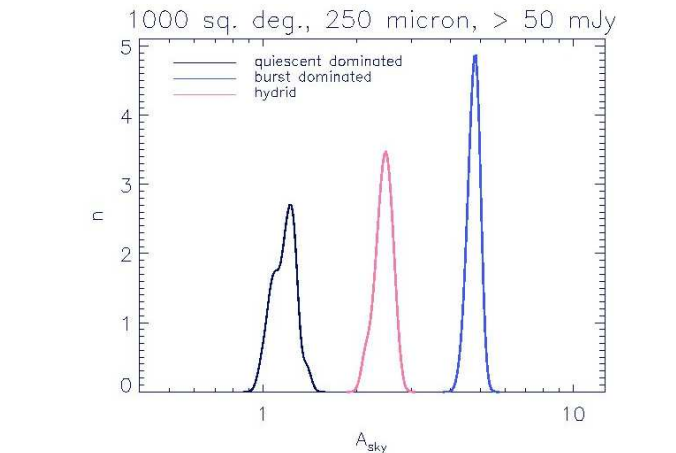


FIG. 12.— A histogram of the amplitude of the angular correlation function (A_{sky}) of H-ATLAS sources for 100 Monte-Carlo realisations for each of three different models of galaxy formation: the hybrid model described by Van Kampen et al. (2005) and two new models (Van Kampen et al. in preparation).

5.6. Galactic Dust Sources

We will use the H-ATLAS to look for dust associated with stars, especially debris disks and dust around stars on the asymptotic giant branch. We will also study the distribution and spectral properties of dust in the interstellar medium. Although the H-ATLAS fields are at high galactic latitudes, in order to minimize the emission from dust within the Galaxy, IRAS images show that there is plenty of dust even at the galactic poles (Figure 13). The H-ATLAS will allow us to study the structure of an interstellar dust on an angular scale $\simeq 10$ times smaller than was possible with IRAS (Miville-Deschenes et al. 2007) and will be possible with Planck, while still having as good sensitivity to large-scale structure as the two other telescopes. The H-ATLAS will also detect the cold dust missed by IRAS.

A more speculative idea is to look for prestellar cores and protostars at high latitudes. Since the dust disks in galaxies are thin, most of the high-latitude dust is within $0.5\ \text{kpc}$. Therefore, we will be able to carry out a search for prestellar cores and protostars in our fields down to surprisingly low mass limits. On the assumption of a dust temperature of $20\ \text{K}$ and a standard gas-to-dust

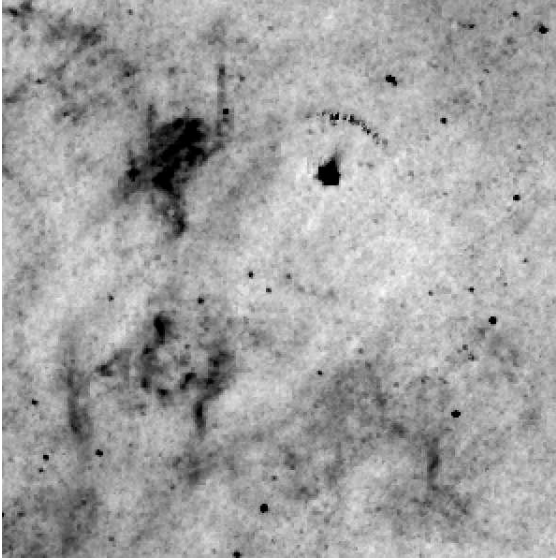


FIG. 13.— IRAS image at $100\ \mu\text{m}$ of a $10 \times 10\ \text{deg}^2$ region around the south galactic pole.

ratio, we estimate that we should detect all protostars and prestellar cores down to a mass of $\sim 0.002 M_{\odot}$ —well below the brown dwarf limit and in the Jupiter regime.

6. FURTHER TECHNICAL DETAILS AND DATA RELEASE

The basic parameters of the survey were given in §2. In this section, we describe some technical issues that will affect the nature of the data that we eventually release to the community.

An important feature of the survey is that we plan to observe all fields twice. The main purpose of this is to overcome the potential problem of low-frequency ($1/f$) noise, caused by either slow drifts in the temperatures of the detectors or other changes in the instrument electronics. These drifts in time can lead to spurious large-scale structure in the final maps, which would be a problem for some of our science projects. As long as the two sets of observations are in different directions, however, it should be possible to use mapping algorithms such as MADmap (Cantalupo et al. 2009) to produce maximum-likelihood images of sky that are free of the effects of this noise. Simulations suggest that as long as the scan direction of the two sets of observations is separated by at least 20 degrees, there should be no features in the final maps caused by these drifts (Waskett et al. 2006).

Achieving two sets of observations with different scan directions, however, is quite tricky, partly because of the severe constraints on the way that Herschel will observe the sky and partly because of the sheer size of H-ATLAS (11% of the time available for open-time key projects). Surveys will be carried out with Herschel by using the telescope to scan across the sky along a great circle, then moving the telescope a short distance in a parallel ‘cross-leg’ direction, and then moving the telescope back along a great circle, thus gradually building up a map of the sky. A complication of observing with SPIRE is that the SPIRE bolometers do not instantaneously fully sample the sky, and so to produce a fully-sampled SPIRE image it is necessary to carry out the scan in one of 24 possible directions that are related to the six-fold symmetry of the array (there is not a similar constraint for PACS

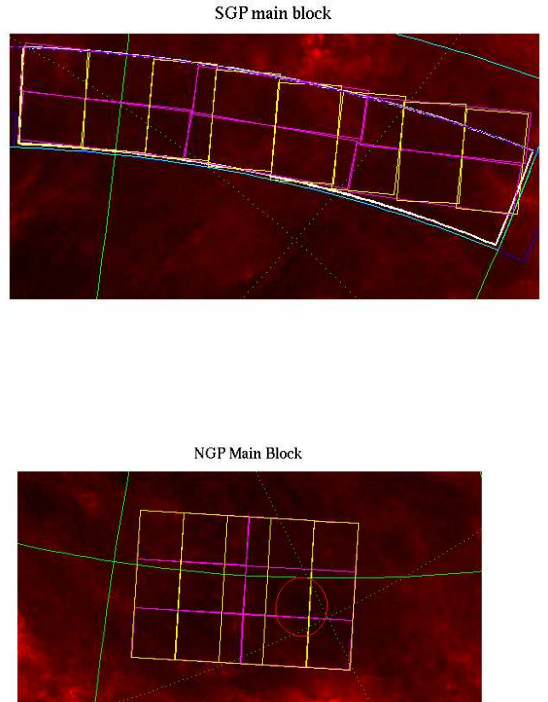


FIG. 14.— The design of the surveys of the ATLAS NGP field and of the larger of the two SGP fields. In both cases, the purple and yellow lines show the areas that will be covered by individual Astronomical Observation Requests (AORs). The other colours outline the areas covered by complementary datasets in other wavebands. The red circle in the NGP figure shows the position of the Coma Cluster.

because it is a fully-sampled array). Other complications are that it is necessary to keep the Sun safely behind the telescope’s sun-shield and that it is only possible to rotate the telescope completely around one axis. Waskett et al. (2007) give a good introduction to the complications of carrying out surveys with Herschel. The result of these constraints is that it is only possible to observe a given field during certain visibility windows, the duration of which depends on the position of the field.

The easiest fields to observe are the GAMA fields, which have long visibility windows because they are the ones closest to the ecliptic plane. The Astronomical Observation Requests (AOR), the units out of which the telescope’s observing programme is built, of the GAMA fields each consist of two sets of observations with orthogonal scan directions of an area of sky $\simeq 4 \times 4\ \text{deg}^2$. These AORs, which will take approximately 16 hours to complete, will result in approximately square images, like those shown in Figure 2, although the orientation of the square will depend on the exact time at which the observation is made. Thus the coverage within each square will be uniform but we cannot predict at the moment the angle that each square will make to the celestial equator, and thus the precise overlap with the area covered by the surveys in other wavebands (§4).

The other two fields are more difficult to observe because they have shorter visibility windows and because we need to map large contiguous areas of sky to make the best use of the complementary data in other wavebands. As an example, we will consider the larger of the

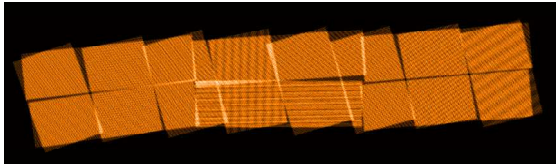


FIG. 15.— A simulation of the likely coverage of the larger of the fields near the south galactic pole. The range of exposure time shown by the colour table is a factor of four.

fields near the south galactic pole (SGP). To make the best use of the redshifts from the 2dF Galaxy Redshift Survey, the field has a small range of declination but a large range of right ascension (Fig. 2). For this field, the individual AORS each contain one set of observations with a single scan direction. Figure 14 shows the layout of the AORs, although their exact orientation depends on exactly when the observations are done. The scan directions are either roughly along lines of constant declination, with the observations covering a rectangular area of $\simeq 3^\circ$ in declination and $\simeq 12^\circ$ in right ascension, or roughly along lines of constant right ascension, with the observations covering a rectangular area of $\simeq 6^\circ$ degrees in declination and $\simeq 4^\circ$ in right ascension. We have set some constraints on when the AORs are observed to avoid the rectangles being rotated too far from a north-south line but it is not possible to make the constraints too severe because of the difficulty of scheduling such a large programme. Fig 15 shows an example of the coverage we are likely to have for this field. The full range of the exposure time shown by the colour table is a factor of four, so the sensitivity in the apparent gaps is a factor of $\simeq 2$ worse than in the places where we have the best coverage. Apart from in these gaps, every point in the field will have at least two sets of observations, with the scans in approximately orthogonal directions, and thus we will be able to use maximum-likelihood imaging algorithms to remove the effect of $1/f$ noise. Figure 14 also shows the design of the AORs for the field near the north galactic pole (NGP). The individual AORS again each contain one set of observations with a single scan direction. There are two sets of AORs with roughly orthogonal scan directions, and each covering a rectangular area of $\simeq 9^\circ \times 4^\circ$ with the longer side in the scan direction. The orientation of the overall field, and the coverage within the field, is still uncertain and will depend on the final telescope schedule. For all the fields, one of the legacy data products will be coverage maps of the fields.

A useful byproduct of our observing strategy of two sets of observations of each point with an field is that we

will be able to look for time-varying and moving objects in the H-ATLAS data. Because of the scheduling difficulties, we have not placed any constraint on the time interval between two observations of the same place within the SGP and NGP fields, and thus it is only within the GAMA fields that we will have two sets of observations separated in time by a roughly constant interval. This interval is approximately 8 hours, which is well-suited for looking for asteroids but not, for example, for objects in the Edgeworth-Kuiper Belt.

We intend to release the H-ATLAS data (maps and catalogues) to the community in a series of data releases. The first data release will be for a $4^\circ \times 4^\circ$ area within the 9-hour GAMA field (Table 1), which will be observed during the Herschel Science Demonstration Phase (October 15th–November 30th 2009). We currently expect to release the maps and catalogues for this region in May 2010. The complexity of telescope scheduling means that we cannot yet give a firm date for the next data release. More information can be found on the Herschel ATLAS website (www.h-atlas.org).

7. CONCLUSIONS

The Herschel ATLAS is the largest open-time key project that will be carried out with the Herschel Space Observatory. It will survey 510 square degrees of the extragalactic sky, four times larger than all the other Herschel surveys combined, in five far-infrared and submillimetre bands. We have described the survey, the complementary multi-wavelength datasets that will be combined with the Herschel data, and the six major science programmes we plan to undertake. Using new models based on a submillimetre survey of nearby galaxies, we have presented predictions of the properties of the sources that will be detected by the H-ATLAS. We intend to release the H-ATLAS data—maps and catalogues—to the astronomical community in a series of data releases. The first of these will be in May 2010.

We thank the UK Science and Technology Facilities Council and the Italian Space Agency (ASI contract I/016/07/0 COFIS) for funding. This research has made use of the NASA/IPAC Extragalactic Database (NED), which is operated by the Jet Propulsion Laboratory, California Institute of Technology, under contract with the National Aeronautics and Space Administration.

REFERENCES

- Amblard, A. and Cooray, A. 2007, *ApJ*, 670, 903
 Baldry, I. et al. 2009, *MNRAS*, submitted
 Balogh, M. et al. 2004, *MNRAS*, 348, 1355
 Bartelmann, M. 2001, *A&A*, 370, 754
 , *A&A*, 388, 732
 Baugh, C. et al. 2005, *MNRAS*, 356, 1191
 Beelen, A. et al. 2006, *ApJ*, 642, 694
 Bendo, G. et al. 2003, *AJ*, 125, 2361
 Bertoldi, F. et al. 2007, *ApJS*, 172, 132
 Bregman, J.N., Snider, B.A., Grego, L. & Cox, C.V. 1998, *ApJ*, 499, 670
 Browne, I. 2003, *MNRAS*, 341, 13
 Cantalup, C., Borrill, J., Jaffe, A., Kisner, T. & Stompor, R. 2009, *astro-ph 0906.1775*
 Cole, S. et al. 2000, *MNRAS*, 319, 168.
 Coleman, G.D., Wu, C.-C. and Weedman, D.W. 1980, *ApJS*, 43, 393
 Colless, M. et al. 2001, *MNRAS*, 328, 1039
 Coppin, K. et al. 2006, *MNRAS*, 372, 1621
 Davies, J. & Burstein, D. (editors) 1995, *The Opacity of Spiral Disks*
 de Zotti, G., Ricci, R., Mesa, D., Silva, L. Mazzotta, P., Toffolatti, L. & Gonzalez-Nuevo, J. 2005, *A&A*, 431, 893
 Devlin, M. et al. 2009, *Nature*, 458, 737.
 Devereux, N. and Young, J.S. 1990, *ApJ*, 359, 42
 Dole, H. et al. 2006, *A&A*, 451, 417
 Driver, S. et al. 2007, *MNRAS*, 379, 1022
 Driver, S. et al. 2009, *Astronomy and Geophysics*, 50, 12
 Driver, S., Popescu, C., Tuffs, R., Graham, A., Liske, J. & Baldry, I. 2008, *ApJ*, 678, 101

- Dunne, L., Eales, S.A., Edmunds, M., Ivison, R., Alexander, P. & Clements, D.L. 2000, MNRAS, 315, 115
- Dunne, L. & Eales, S. 2001, MNRAS, 327, 697
- Dunne, L., Eales, S. & Edmunds, M. 2003, MNRAS, 341, 589.
- Dwek, E. et al. 1998, ApJ, 508, 106
- Dye, S., Smail, I., Swinbank, A., Ebeling, H. & Edge, A. 2007a, MNRAS, 379, 308
- Dye, S. et al. 2007b, MNRAS, 375, 725
- Dye, S. et al. 2009, ApJ, in press
- Eales, S.A. et al. 1999, ApJ, 515, 518
- Eales, S.A. et al. 2009, ApJ, submitted
- Eddington, A. 1940, MNRAS, 100, 354
- Fixsen, D.J., Dwek, E., Mather, J.C., Bennett, C.L. & Shafer, R.A., ApJ, 508, 123
- Greve, T.R., Ivison, R.J., Bertoldi, F., Dunlop, J.S., Lutz, D. & Carilli, C.L. 2004, MNRAS, 354, 779.
- Greve, T.R., Pope, A., Scott, D., Ivison, R.J., Conselice, C.J. & Bertoldi, F. 2008, MNRAS, in press
- Griffin, M. et al. 2007, Advances in Space Research, 40, 612
- Frayser, D.T. et al. 2006, AJ, 131, 250
- Frayser, D.T. et al. 2006, ApJ, 647, L9
- Haas, M. et al. 2003, A&A, 402, 87
- Heavens, A., Panter, B., Jimenez, R. & Dunlop, J. 2004, Nature, 428, 625.
- Helou, G., Rowan-Robinson, M. & Helou, G. 1986, ApJ, 298, L7
- Holmberg, E. 1958, Medd. Lund. Astron. Obs. Ser. 2, 6
- Hughes, D. et al. 1998, Nature, 394, 241
- Ibar, E. et al. 2009, MNRAS, 386, 953
- Jester, S. et al. 2005, AJ, 130, 873
- Johnstone, S. et al. 2007, PASA, 24, 174
- Kashlinsky, A. & Atrio-Barandela, F. 2000, ApJ, 536, L67
- Kauffmann, G. et al. 2003a, MNRAS, 341, 33
- Kauffmann, G. et al. 2003b, MNRAS, 341, 54
- Kauffmann, G. et al. 2004, MN, 353, 713
- Keller, S., Schmidt, B.P. & Bessell, M.S. 2007, Proceedings of the ESO Calibration Workshop, astro-ph 0704.1339
- Lagache, G., Dole, H. & Puget, J.-L. 2003, MNRAS, 338, 555.
- Lagache, G. et al. 2004, ApJS, 154, 112
- Lagache, G. et al. 2007, ApJ, 665, L89
- Lewis, I. et al. 2002, MNRAS, 334, 673
- Loveday, J. et al. 2004, MN, 347, 601
- Magorrian, J. et al. 1998, AJ, 115, 2285
- Maddox, S., Efstathiou, G. & Sutherland, W. 1990, MNRAS, 246, 433
- Mivilles-Deschenes, M.-A. et al. 2007, A&A, 459, 595
- Negrello, M. et al. 2007, MNRAS, 377, 1557
- Obric, M. et al. 2006, MNRAS, 370, 1677
- Oliver, S. et al. in preparation
- Perera, T.A. et al. 2008, MNRAS, submitted
- Poglitsch, A. et al. 2006, SPIE, 6265, 8
- Priddey, R. et al. 2003, MNRAS, 339, 1183
- Saunders, W. et al. 1990, MN, 242, 318
- Scott, S. et al. 2002, MNRAS, 331, 817
- Scott, K.S. et al. 2008, MNRAS, 385, 2225
- Serjeant, S. & Hatziminaoglou, E. 2009, MNRAS, 397, 265
- Smail, I., Ivison, R. & Blain, A. 1997, ApJ, 490, L5
- Strauss, M. et al. 2002, AJ, 124, 1810
- Takeuchi, T.T., Ishii, T.T., Dole, H., Dennefeld, M., Lagache, G. & Puget, J.-L. 2006, A&A, 448, 525
- Van Kampen, E. et al. 2005, MNRAS, 359, 469
- Vlahakis, C., Dunne, L. & Eales, S. 2005, MNRAS, 364, 1253
- Vlahakis, C., Dunne, L. & Eales, S. 2007, MNRAS, 379, 1042
- Warren, S. et al. 2007, astro-ph 0703037.
- Waskett, T.J., Sibthorpe, B., Griffin, M.J. & Chaniai, P.F. 2007, MNRAS, 381, 1583
- Waskett, T.J., Sibthorpe, B. & Griffin, M.J. 2006, Studying Galaxy Evolution with Spitzer and Herschel, astro-ph 0609783
- York, D.G. et al. 2000, AJ, 120, 1579
- Zemcov, M. et al. 2007, MNRAS, 376, 1073